Frustrated magnetism of spin-$\frac{1}{2}$ Heisenberg diamond and octahedral chains as a statistical mechanical monomer-dimer problem

Jozef Strečka [1,*] Taras Verkholyak [2] Johannes Richter [3,4] Katarína Karl'ová [1] Oleg Derzhko [2] and Jürgen Schnack [5]

[1]*Department of Theoretical Physics and Astrophysics, Faculty of Science, P. J. Šafárik University, Park Angelinum 9, 04001 Košice, Slovakia*

[2]*Institute for Condensed Matter Physics, NASU, Svientsitskii Street 1, 79011 L'viv, Ukraine*

[3]*Institut für Physik, Otto-von-Guericke Universität in Magdeburg, 39016 Magdeburg, Germany*

[4]*Max-Planck-Institut für Physik Komplexer Systeme, 01187 Dresden, Germany*

[5]*Department of Physics, Bielefeld University, P.O. Box 100131, D-33501 Bielefeld, Germany*

(Received 26 October 2021; revised 21 January 2022; accepted 27 January 2022; published 15 February 2022)

It is evidenced that effective lattice-gas models of hard-core monomers and dimers afford a proper description of low-temperature features of spin-$\frac{1}{2}$ Heisenberg diamond and octahedral chains. In addition to monomeric particles assigned within the localized-magnon theory to bound one- and two-magnon eigenstates, the effective monomer-dimer lattice-gas model includes dimeric particles assigned to a singlet-tetramer (singlet-hexamer) state as a cornerstone of dimer-tetramer (tetramer-hexamer) ground state of a spin-$\frac{1}{2}$ Heisenberg diamond (octahedral) chain. The feasibility of the effective description is confirmed through the exact diagonalization and finite-temperature Lanczos methods. Both quantum spin chains display rich ground-state phase diagrams including discontinuous as well as continuous field-driven phase transitions, whereby the specific heat shows in vicinity of the former phase transitions an extraordinary low-temperature peak coming from a highly degenerate manifold of low-lying excitations.

DOI: 10.1103/PhysRevB.105.064420

I. INTRODUCTION

Frustrated quantum Heisenberg spin systems have remained for a long time at the forefront of research interest because they often exhibit intriguing ordered or disordered quantum ground states in addition to unconventional magnetic properties emergent at sufficiently low temperatures [1,2]. From this perspective, it is quite bizarre that a more complex nature of exchange pathways initiating geometric spin frustration simultaneously offers a genuine possibility of finding quantum ground states of frustrated Heisenberg spin models by the use of rigorous methods. Among a few highly celebrated examples of frustrated quantum Heisenberg spin models with exactly known ground states, one could, for instance, mention the zigzag ladder [3], the Shastry-Sutherland lattice [4], the delta chain [5], and the one-dimensional chain of linked tetrahedra [6].

Compared with this, it is generally much more difficult to cope with magnetic and thermodynamic properties of frustrated quantum Heisenberg spin models at low but nonzero temperatures. The unbiased exact diagonalization (ED) [7,8] or finite-temperature Lanczos method (FTLM) [9–14] are regrettably limited to relatively small finite-sized Heisenberg spin systems involving at most a few dozen quantum spins. On the other hand, the large-scale simulations of frustrated Heisenberg spin models based on quantum Monte Carlo (QMC) methods suffer from a serious negative-sign problem when performed in a standard basis, and one should accordingly resort to more challenging sign-problem-free QMC computations performed in a dimer [15–19] or trimer [20] basis.

A flat band emergent in the one-magnon spectrum of frustrated Heisenberg spin systems bears evidence of a magnon, which is bound to a small portion of the frustrated spin lattice due to a destructive quantum interference. Owing to this fact, the many-magnon eigenstates of frustrated Heisenberg spin models can be simply designed from a bound one-magnon eigenstate within the concept of localized magnons establishing an effective lattice-gas model [21], which consists of an independent arrangement of bound magnons on trapping cells of frustrated spin lattices [22–24].

It should be pointed out, however, that the effective lattice-gas models developed within the standard formulation of the localized-magnon theory are usually eligible for a description of frustrated quantum Heisenberg spin systems only in a high-field region sufficiently close to the saturation field [22–24]. One may fortunately avoid this shortcoming in a special subclass of the frustrated quantum Heisenberg spin models satisfying local spin-conservation laws. It has been verified that an additional counting of the lowest-energy bound two-magnon eigenstate paves the way toward a complete description of low-temperature magnetization curves and thermodynamics of highly frustrated Heisenberg octahedral chains from zero up to the saturation field [25–28].

In this paper, we generalize the localized-magnon theories established previously for the spin-$\frac{1}{2}$ Heisenberg diamond and octahedral chains by extending their validity to a less

*jozef.strecka@upjs.sk

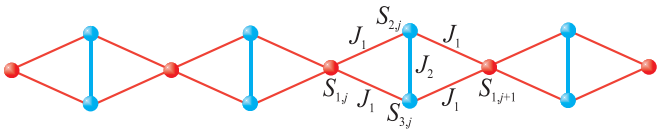

FIG. 1. A schematic illustration of the spin-$\frac{1}{2}$ Heisenberg diamond chain including the notation for the lattice sites and assumed coupling constants.

frustrated parameter space including dimer-tetramer [29] and tetramer-hexamer (TH) [25] ground states, respectively. It is worthwhile to remark that the spin-$\frac{1}{2}$ Heisenberg diamond chain bears a close relation to several copper-based magnetic compounds such as azurite $Cu_3(CO_3)_2(OH)_2$ [30,31], $A_3Cu_3AlO_2(SO_4)_4$ (A = K, Rb, and Cs) [32–34], $[Cu_3(OH)_2(CH_3COO)(H_2O)_4](RSO_3)_2$ (RSO_3 = organic sulfonate anions) [35], and $Cu_3(CH_3COO)_4(OH)_2 \cdot 5H_2O$ [36]. Although we do not have at present any knowledge about a possible experimental realization of the spin-$\frac{1}{2}$ Heisenberg octahedral chain, a relatively numerous family of hexanuclear complexes with the magnetic core of a discrete copper-based octahedron $\{Cu_6\}$ [37–40] could be used for a brick-and-mortar synthesis of a one-dimensional copper polymeric chain of corner-sharing octahedra. A closely related extended magnetic structure with the architecture of a three-dimensional network of corner-sharing octahedra $\{Cu_6\}$ is, for instance, realized in the copper-based metal-organic framework $[Cu_3(tpt)_4](ClO_4)_3$ [41]. Last but not least, an artificial design of the spin-$\frac{1}{2}$ Heisenberg octahedral chain achieved through magnetic atom-trap lattices is also feasible with regard to a recent successful realization of several related one-dimensional magnetic structures such as ladders and diamond spin chains [42].

The outline of this paper is as follows. The overall ground-state phase diagrams of the spin-$\frac{1}{2}$ Heisenberg diamond and octahedral chains will be presented in Secs. II and IV together with a few basic steps elucidating its construction from exact and density-matrix renormalization group (DMRG) calculations of the effective mixed-spin Heisenberg chains. The spin-$\frac{1}{2}$ Heisenberg diamond and octahedral chains are reformulated within the modified localized-magnon theory, establishing their connection to a one-dimensional lattice-gas model of hard-core monomers and dimers, in Secs. III and V, where an eligibility of the effective description is also corroborated through a detailed comparison with numerical data obtained from the full ED and FTLM. The paper ends with a brief summary of the most important findings in Sec. VI, where a few future outlooks are also presented.

II. GROUND STATES OF A SPIN-$\frac{1}{2}$ HEISENBERG DIAMOND CHAIN

First, let us consider the spin-$\frac{1}{2}$ Heisenberg diamond chain, which is schematically illustrated in Fig. 1 and mathematically defined through the Hamiltonian:

$$\hat{\mathcal{H}} = \sum_{j=1}^{N} \left[J_1(\hat{\mathbf{S}}_{1,j} + \hat{\mathbf{S}}_{1,j+1}) \cdot (\hat{\mathbf{S}}_{2,j} + \hat{\mathbf{S}}_{3,j}) + J_2 \hat{\mathbf{S}}_{2,j} \cdot \hat{\mathbf{S}}_{3,j} - h \sum_{i=1}^{3} \hat{S}^z_{i,j} \right], \tag{1}$$

where $\hat{\mathbf{S}}_{i,j}$ ($i = 1, 2, 3$; $j = 1, \ldots, N$) denotes the spin-$\frac{1}{2}$ operator assigned to a lattice site unambiguously given by two subscripts; the first subscript specifies spins from a given unit cell, and the second subscript determines the unit cell itself. The coupling constant $J_1 > 0$ stands for the antiferromagnetic interaction between nearest-neighbor monomeric ($S_{1,j}$) and dimeric ($S_{2,j}$, $S_{3,j}$) spins, while the coupling constant $J_2 > 0$ accounts for the antiferromagnetic intradimer interaction being responsible for a geometric spin frustration. The Zeeman term $h \geqslant 0$ accounts for an effect of the external magnetic field, and finally, the periodic boundary condition is imposed for simplicity $S_{1,N} \equiv S_{1,1}$.

The ground-state phase diagram of the spin-$\frac{1}{2}$ Heisenberg diamond chain given by the Hamiltonian in Eq. (1) can be obtained by combining three complementary techniques. One may adapt variational arguments (see Appendix in Ref. [43]) to rigorously prove, in the highly frustrated parameter region $J_2 > 2J_1$ and low enough magnetic fields $h < J_1 + J_2$, the monomer-dimer (MD) ground state schematically illustrated in Fig. 2 and mathematically given by the eigenvector:

$$|\mathrm{MD}\rangle = \begin{cases} \prod_{j=1}^{N} |S_{1,j}\rangle \otimes \frac{1}{\sqrt{2}}(|\uparrow_{2,j}\downarrow_{3,j}\rangle - |\downarrow_{2,j}\uparrow_{3,j}\rangle), & h = 0, \\ \prod_{j=1}^{N} |\uparrow_{1,j}\rangle \otimes \frac{1}{\sqrt{2}}(|\uparrow_{2,j}\downarrow_{3,j}\rangle - |\downarrow_{2,j}\uparrow_{3,j}\rangle), & h > 0, \end{cases} \tag{2}$$

where $|S_{1,j}\rangle$ denotes any out of two available states $|\uparrow_{1,j}\rangle$ and $|\downarrow_{1,j}\rangle$ of the monomeric spins. It is worthwhile to remark that the MD ground state in Eq. (2) is macroscopically degenerate at zero magnetic field due to the frustrated (paramagnetic) character of all monomeric spins $S_{1,j}$, which are consequently perfectly aligned into the magnetic-field direction once the external field is turned on. Another independent confirmation of the MD ground state in Eq. (2) is provided by the localized-magnon approach, which restricts its presence in the highly frustrated parameter space $J_2 > 2J_1$ to sufficiently low magnetic fields $h < h_s$ not exceeding the saturation field $h_s = J_1 + J_2$ associated with a field-driven phase transition to the fully saturated ferromagnetic phase [23,44,45]. It could be thus concluded that the variational and localized-magnon

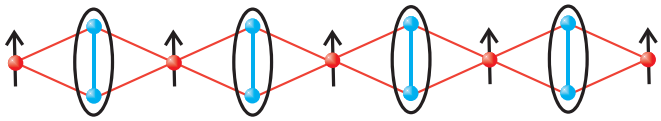

FIG. 2. A schematic illustration of the monomer-dimer ground state given in Eq. (2), which is responsible for occurrence of intermediate $\frac{1}{3}$ plateau in a zero-temperature magnetization curve. An oval denotes a singlet-dimer state.

theories give evidence of the MD ground state in Eq. (2) from zero up to the saturation field in the highly frustrated parameter region $J_2 > 2J_1$.

In the rest of the parameter space $J_2 < 2J_1$, the ground states of the spin-$\frac{1}{2}$ Heisenberg diamond chain cannot be simply found on the grounds of exact analytical calculations. To this end, it is convenient to rewrite the zero-field part of the Hamiltonian in Eq. (1) into the following equivalent form:

$$\hat{\mathcal{H}} = J_1 \sum_{j=1}^{N} (\hat{\mathbf{S}}_{1,j} + \hat{\mathbf{S}}_{1,j+1}) \cdot \hat{\mathbf{S}}_{c,j} + \frac{J_2}{2} \sum_{j=1}^{N} \left(\hat{\mathbf{S}}_{c,j}^2 - \frac{3}{2} \right), \tag{3}$$

which directly implies a local conservation of the composite spin $\hat{\mathbf{S}}_{c,j} = \hat{\mathbf{S}}_{2,j} + \hat{\mathbf{S}}_{3,j}$ on vertical dimers of a spin-$\frac{1}{2}$ Heisenberg diamond chain. The composite spin on vertical dimers is accordingly a conserved quantity with well-defined quantum spin numbers $S_{c,j} = 0$ or 1. Hence, it follows that all ground states of the spin-$\frac{1}{2}$ Heisenberg diamond chain can be derived from the lowest-energy eigenstates of effective mixed spin-$(\frac{1}{2}, S_{c,j})$ Heisenberg chains schematically illustrated in Fig. 3 when performing an appropriate shift of their eigenenergies according to the second term of the Hamiltonian in Eq. (3). Note furthermore that the z component of the total spin operator $\hat{S}_T^z = \sum_{j=1}^{N} \sum_{i=1}^{3} \hat{S}_{i,j}^z$ commutes with the Hamiltonian in Eq. (1), which means that most preferable energy eigenvalues of the spin-$\frac{1}{2}$ Heisenberg diamond chain in a nonzero magnetic field directly follow from their zero-field counterparts when performing only a trivial shift by the respective Zeeman's term:

$$E\left(S_T^z, h \neq 0\right) = E\left(S_T^z, h = 0\right) - hS_T^z. \tag{4}$$

Although one should generally find out lowest-energy eigenstates of effective mixed spin-$(\frac{1}{2}, S_{c,j})$ Heisenberg chains in Eq. (3) with all possible combinations of the composite spins ($\forall j\ S_{c,j} = 0$ or 1), it is often sufficient to consider only a few particular cases with quantum spin numbers that do not break translational symmetry or at most limit the spontaneous breaking of translational symmetry to a few unit cells.

A comprehensive analysis of the ground-state phase diagram of the spin-$\frac{1}{2}$ Heisenberg diamond chain in zero field

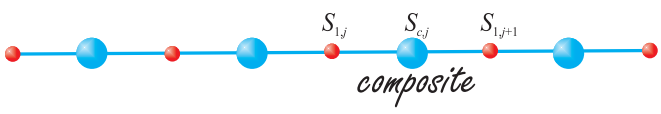

FIG. 3. A schematic illustration of the effective mixed spin-$(\frac{1}{2}, S_{c,j})$ Heisenberg chains, in which the composite spins may acquire the values $S_{c,j} = 0$ or 1 for a diamond chain and $S_{c,j} = 0$, 1, or 2 for an octahedral chain.

was performed in Ref. [29]. It was proven that all its ground states stem from the effective mixed spin-$(\frac{1}{2}, 0)$ or mixed spin-$(\frac{1}{2}, 1)$ Heisenberg chains without translationally broken symmetry or the effective mixed spin-$(\frac{1}{2}, 1, \frac{1}{2}, 0)$ Heisenberg chain with a period doubling. In Appendix A, we prove that this property is preserved also in nonzero fields.

The lowest-energy eigenstate of the effective mixed spin-$(\frac{1}{2}, 0)$ Heisenberg chain with the unique choice of zero composite spin $\forall j\ S_{c,j} = 0$ naturally corresponds to the MD ground state in Eq. (2) with the exact energy:

$$E_{1/2-0}\left(N, S_T^z = \frac{N}{2}\right) = -\frac{3}{4}NJ_2 - \frac{1}{2}Nh, \tag{5}$$

because the singlet-dimer state at vertical bonds assigned to zero composite spin decouples all correlations between the dimeric and monomeric spins. It is worthwhile to remark, moreover, that the effective mixed-spin Heisenberg chains with regularly alternating zero composite spins are always fragmented into smaller quantum spin clusters, for which the lowest-energy eigenstates can be rather easily calculated by the ED method. On the other hand, the fragmentation does not occur for the other unique choice of the composite spins $\forall j\ S_{c,j} = 1$, which contrarily gives rise to highly correlated collective eigenstates with the energy eigenvalues governed by the formula:

$$E_{1/2-1}\left(N, S_T^z\right) = NJ_1 \varepsilon_{1/2-1}\left(N, S_T^z\right) + \tfrac{1}{4}NJ_2 - hS_T^z, \tag{6}$$

where $\varepsilon_{1/2-1}(N, S_T^z)$ denotes the energy per unit cell of the effective mixed spin-$(\frac{1}{2}, 1)$ Heisenberg chain with unit coupling constant, the number of unit cells N, and z component of the total spin S_T^z. The mixed spin-$(\frac{1}{2}, 1)$ Heisenberg chain exhibits at low enough magnetic fields the gapped ferrimagnetic phase with a z component of the total spin $S_T^z = (1 - \frac{1}{2}) \times N = N/2$ due to ordering of energy levels imposed by the Lieb-Mattis theorem [46], whereby the eigenstates with higher values of the total spin momentum $S_T^z > N/2$ form a continuous band pertinent to the gapless Tomonaga-Luttinger quantum spin liquid emergent at higher magnetic fields when an energy gap above the Lieb-Mattis ferrimagnetic phase closes [47–51]. To gain the respective eigenenergies $\varepsilon_{1/2-1}(N, S_T^z)$ of the effective mixed spin-$(\frac{1}{2}, 1)$ Heisenberg chain, one has to resort to state-of-the-art numerical calculations. To this end, we have implemented DMRG simulations of the effective mixed spin-$(\frac{1}{2}, 1)$ Heisenberg chain with up to 120 spins ($N = 60$ unit cells, which correspond to the diamond chain of 180 spins) within the open-source software Algorithms and Libraries for Physics Simulation (ALPS) project [52]. Finally, another available ground state relates to the lowest-energy eigenstate of the effective mixed spin-$(\frac{1}{2}, 1, \frac{1}{2}, 0)$ Heisenberg chain, where singlet and polarized triplet states regularly alternate on vertical dimers. The singlet-dimer states break the effective mixed spin-$(\frac{1}{2}, 1, \frac{1}{2}, 0)$ Heisenberg chain into noninteracting three-spin clusters, which also turn out to be in the singlet state within the lowest-energy eigenstate with the energy:

$$E_{1/2-1-1/2-0}\left(N, S_T^z = 0\right) = -\tfrac{1}{4}NJ_2 - NJ_1. \tag{7}$$

This lowest-energy eigenstate thus corresponds to the singlet tetramer-dimer (TD) phase of the spin-$\frac{1}{2}$ Heisenberg diamond chain, which is schematically depicted in Fig. 4 and mathematically given by the eigenvector:

$$|\mathrm{TD}\rangle = \prod_{j=1}^{N/2} \frac{1}{\sqrt{3}}\Big[|\uparrow_{1,2j-1}\downarrow_{2,2j-1}\uparrow_{3,2j-1}\downarrow_{1,2j}\rangle + |\downarrow_{1,2j-1}\uparrow_{2,2j-1}\downarrow_{3,2j-1}\uparrow_{1,2j}\rangle - \frac{1}{2}(|\uparrow_{1,2j-1}\uparrow_{2,2j-1}\downarrow_{3,2j-1}\downarrow_{1,2j}\rangle + |\uparrow_{1,2j-1}\downarrow_{2,2j-1}\downarrow_{3,2j-1}\uparrow_{1,2j}\rangle + |\downarrow_{1,2j-1}\uparrow_{2,2j-1}\uparrow_{3,2j-1}\downarrow_{1,2j}\rangle + |\downarrow_{1,2j-1}\downarrow_{2,2j-1}\uparrow_{3,2j-1}\uparrow_{1,2j}\rangle)\Big] \otimes \frac{1}{\sqrt{2}}(|\uparrow_{2,2j}\downarrow_{3,2j}\rangle - |\downarrow_{2,2j}\uparrow_{3,2j}\rangle). \tag{8}$$

Note that the singlet TD phase is twofold degenerate because another linearly independent eigenstate with the same energy can be obtained from the eigenvector in Eq. (8) by interchanging singlet-tetramer and singlet-dimer states on odd and even unit cells. The TD phase emerges only if the interaction ratio is from the interval $0.91 < J_2/J_1 < 2.0$ and the magnetic field is sufficiently small $h/J_1 < 0.55$, whereby the highest possible field value for existence of the TD ground state is achieved for $J_2/J_1 \approx 1.45$, see Fig. 5.

The ground-state phase diagram constructed from all previously described lowest-energy eigenstates of the spin-$\frac{1}{2}$ Heisenberg diamond chain is depicted in Fig. 5 in the interaction ratio vs magnetic field plane. In total, the displayed phase diagram involves five different ground states: the gapped Lieb-Mattis ferrimagnetic phase, the gapless Tomonaga-Luttinger quantum spin liquid, the fully polarized ferromagnetic phase, the MD phase, and the TD phase. Two horizontal phase boundaries delimiting the Tomonaga-Luttinger quantum spin liquid mark continuous field-driven quantum phase transitions, while all other phase boundaries denote discontinuous field-driven phase transitions accompanied with discontinuous magnetization jumps. The magnetization corresponding to the ferrimagnetic phase and the MD phase equals $\frac{1}{3}$ of the saturation magnetization, while the TD phase has zero magnetization owing to the singlet character of regularly alternating singlet tetramers and singlet dimers. Contrary to this, the magnetization of the Tomonaga-Luttinger quantum spin liquid continuously rises upon increasing of the magnetic field due to the gapless character of this quantum ground state. The overall ground-state phase diagram of the symmetric spin-$\frac{1}{2}$ Heisenberg diamond chain is lacking in the literature, while the zero-field phase boundaries between the ferrimagnetic, TD, and MD phases are in perfect agreement with the former results reported by Takano *et al.* [29].

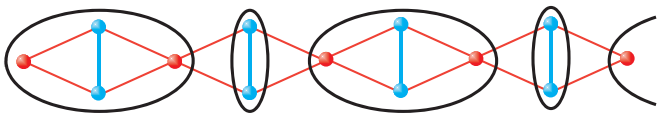

FIG. 4. A schematic illustration of the singlet tetramer-dimer phase given by the eigenvector in Eq. (8). Large and small ovals represent regularly alternating singlet-tetramer and singlet-dimer states.

III. HEISENBERG DIAMOND CHAIN AS MD PROBLEM

In this section, we will turn our attention to a description of low-temperature magnetization curves and thermodynamics of the spin-$\frac{1}{2}$ Heisenberg diamond chain. It is noteworthy that the standard localized-magnon theory based on a classical lattice-gas model of hard-core monomers offers a satisfactory description of low-temperature magnetothermodynamics of the spin-$\frac{1}{2}$ Heisenberg diamond chain only in the highly frustrated parameter region $J_2/J_1 > 2$ [23,44,45], whereas our aim is to proceed beyond this simple theory. The low-energy features of the spin-$\frac{1}{2}$ Heisenberg diamond chain will be effectively described by the one-dimensional lattice-gas model of hard-core monomers and dimers, which will allow us to extend the range of validity of the localized-magnon approach to a less frustrated parameter space involving the singlet TD phase in Eq. (8). The MD lattice-gas model defined on an auxiliary one-dimensional lattice includes hard-core monomeric particles assigned to the singlet-dimer states on vertical bonds:

$$|m\rangle_j = \frac{1}{\sqrt{2}}(|\uparrow_{2,j}\downarrow_{3,j}\rangle - |\downarrow_{2,j}\uparrow_{3,j}\rangle), \tag{9}$$

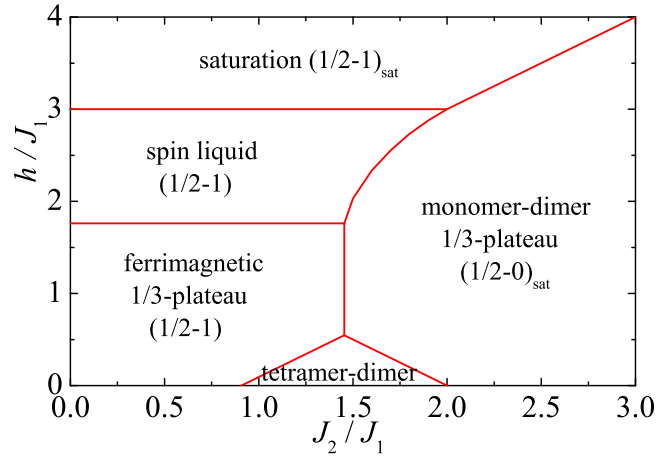

FIG. 5. The ground-state phase diagram of the spin-$\frac{1}{2}$ Heisenberg diamond chain in the $J_2/J_1 - h/J$ plane. The numbers in parentheses determine spin values within the effective mixed spin-($\frac{1}{2}$, S_c) Heisenberg chain.

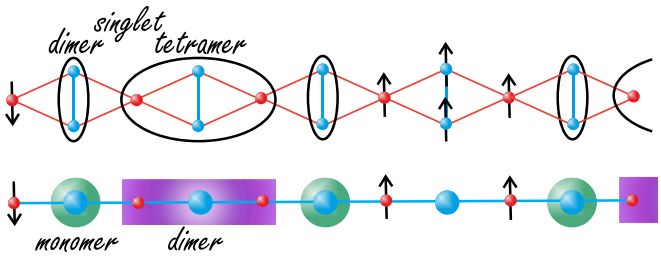

FIG. 6. One typical permissible state of the spin-$\frac{1}{2}$ Heisenberg diamond chain and its equivalent representation within the two-component lattice-gas model of hard-core monomers and dimers. Small red spheres of the auxiliary lattice correspond to the monomeric spins $S_{1,j}$, while large blue spheres of the auxiliary lattice correspond to the composite spins $S_{c,j}$ assigned to the vertical dimers $S_{2,j} - S_{3,j}$.

as well as hard-core dimeric particles assigned to the singlet-tetramer states of diamond (four-spin) clusters being a cornerstone of the TD ground state in Eq. (8):

$$|d\rangle_j = \frac{1}{\sqrt{3}}(|\uparrow_{1,j}\downarrow_{2,j}\uparrow_{3,j}\downarrow_{1,j+1}\rangle + |\downarrow_{1,j}\uparrow_{2,j}\downarrow_{3,j}\uparrow_{1,j+1}\rangle) - \frac{1}{\sqrt{12}}(|\uparrow_{1,j}\uparrow_{2,j}\downarrow_{3,j}\downarrow_{1,j+1}\rangle + |\uparrow_{1,j}\downarrow_{2,j}\downarrow_{3,j}\uparrow_{1,j+1}\rangle + |\downarrow_{1,j}\uparrow_{2,j}\uparrow_{3,j}\downarrow_{1,j+1}\rangle + |\downarrow_{1,j}\downarrow_{2,j}\uparrow_{3,j}\uparrow_{1,j+1}\rangle). \tag{10}$$

One typical permissible state of the spin-$\frac{1}{2}$ Heisenberg diamond chain and its equivalent representation within the developed MD lattice-gas model is displayed in Fig. 6. Small red circles of the auxiliary lattice correspond to lattice sites of the monomeric spins $S_{1,j}$, and large blue circles of the auxiliary lattice correspond to lattice positions of the composite spins $S_{c,j} = S_{2,j} + S_{3,j}$ of the vertical dimers. The composite spins corresponding to the vertical dimers are accessible to the fully polarized ferromagnetic state acting as a reference vacuum state, the singlet-dimer state in Eq. (9), represented by a monomeric particle schematically shown by a large green circle, and the singlet-tetramer state in Eq. (10), represented by a dimeric particle (large violet rectangle) incorporating two enclosing monomeric spins $S_{1,j}$ and $S_{1,j+1}$ as well. If the energy is defined relative to the fully polarized ferromagnetic state serving as a reference state, then one should assign the chemical potential $\mu_1 = J_1 + J_2 - h$ to the monomeric particles connected with the singlet-dimer state in Eq. (9) and the chemical potential $\mu_2 = 3J_1 - h$ to the dimeric particles associated with the singlet-tetramer state in Eq. (10). The effective Hamiltonian of the one-dimensional lattice-gas model of hard-core monomers and dimers consequently reads

$$\mathcal{H}_{\rm eff} = E^0_{\rm FM} - h\sum_{j=1}^{N}\left[1 + S^z_{1,j}(1-d_{j-1})(1-d_j)\right] - \mu_1\sum_{j=1}^{N} m_j - \mu_2\sum_{j=1}^{N} d_j, \tag{11}$$

where $E^0_{\rm FM} = NJ_1 + NJ_2/4$ refers to the zero-field energy of the fully polarized ferromagnetic state, the second term is the respective Zeeman's energy, and $m_j = 0, 1$ and $d_j = 0, 1$ are occupation numbers of the hard-core monomeric and dimeric particles, respectively. The partition function of the MD lattice-gas model defined through the Hamiltonian in Eq. (11) can be written in the compact form:

$$\mathcal{Z} = \exp\big(-\beta E^0_{\rm FM}\big)\sum_{\{S^z_{1,j}\}}\sum_{\{m_j\}}\sum_{\{d_j\}}\prod_{j=1}^{N}\frac{1}{4^{d_j}}(1-d_{j-1}d_j)(1-m_jd_j) \times \exp\big\{\beta\big[\mu_1 m_j + \mu_2 d_j + hS^z_{1,j}(1-d_{j-1})(1-d_j)\big]\big\}. \tag{12}$$

Here, $\beta = 1/(k_{\rm B}T)$, where $k_{\rm B}$ is the Boltzmann constant, T is absolute temperature, the summation $\sum_{\{S^z_{1,j}\}}$ runs over spin states of all monomeric spins $S_{1,j}$, and the summations $\sum_{\{m_j\}}$ and $\sum_{\{d_j\}}$ are carried out over all possible values of the respective occupation numbers. The factor $(1 - d_{j-1}d_j)(1 - m_jd_j)$ ensures a hard-core constraint forbidding overlap and/or double occupancy of auxiliary lattice sites by the monomeric and dimeric particles, while the factor $\frac{1}{4^{d_j}}$ is the correction term for the singlet-tetramer state in Eq. (10) that would be accounted four times without this factor when one performs the summation over spin states of two monomeric spins $S_{1,j}$ and $S_{1,j+1}$. The important feature of the partition function in Eq. (12) is the possibility to sum over all the states of the monomeric spins $S_{1,j}$ and hard-core monomer particles m_j independently. In fact, the complete hard-core conditions between the quasiparticles should also include the projection operator $[1 - (1 - m_i)d_{i+1}][1 - d_i(1 - m_{i+1})]$, which ensures that the singlet-plaquette state (d_i particle) cannot be followed by the fully polarized state on the adjacent dimer. The energy of the latter state is much larger than the energy scale of allowed states present in the effective Hamiltonian in Eq. (11), and for simplicity, it can be completely left out from consideration. After performing the summations $\sum_{\{S^z_{1,j}\}}$ and $\sum_{\{m_j\}}$, the expression behind the product symbol can be expressed solely in terms of the occupation numbers of the dimeric particles:

$$T(d_j, d_{j+1}) = \frac{1}{4^{d_j}}(1-d_{j-1}d_j)2\exp(\beta h + \beta\mu_2 d_j) \times [1 + (1-d_j)\exp(\beta\mu_1)] \times \cosh\left[\frac{\beta h}{2}(1-d_{j-1})(1-d_j)\right]. \tag{13}$$

The expression in Eq. (13) can be in turn identified as the transfer matrix, which allows a simple calculation of the partition function in Eq. (12) within the transfer-matrix method [53] exploiting a consecutive summation over the occupation numbers of the dimeric particles:

$$\mathcal{Z} = \exp\big(-\beta E^0_{\rm FM}\big)\sum_{\{d_j\}}\prod_{j=1}^{N} T(d_{j-1}, d_j) = \exp\big(-\beta E^0_{\rm FM}\big){\rm Tr}T^N = \exp\big(-\beta E^0_{\rm FM}\big)(\lambda_+^N + \lambda_-^N). \tag{14}$$

The final expression for the partition function in Eq. (14) is given through two eigenvalues $\lambda_\pm$ obtained after a straightforward diagonalization of the two-by-two transfer matrix in

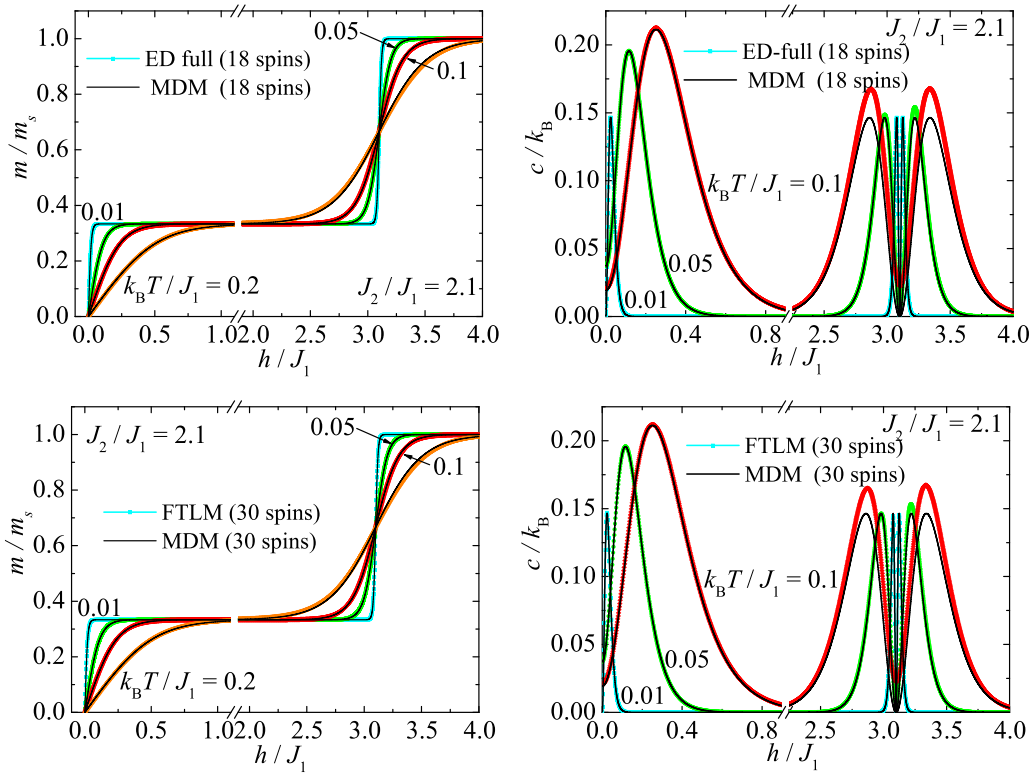

FIG. 7. (Left panel) Magnetization curves of the spin-$\frac{1}{2}$ Heisenberg diamond chain with $J_2/J_1 = 2.1$ obtained from the effective monomer-dimer model (MDM) vs the exact diagonalization (ED) data for 18 spins (upper panel) and the finite-temperature Lanczos method (FTLM) data for 30 spins (lower panel) of the original model in Eq. (1). (Right panel) The same as in the left panel but for the specific heat. Thin black lines show analytical results derived from the effective MDM in Eq. (11), while colored symbols refer to the ED (upper panel) or FTLM (lower panel). Note that there is an axis break in the middle of the intermediate $\frac{1}{3}$-plateau.

Eq. (13):

$$\lambda_{\pm} = e^{\beta h}\left\{\cosh\left(\frac{\beta h}{2}\right)\Xi_d \pm \sqrt{\left[\cosh\left(\frac{\beta h}{2}\right)\Xi_d\right]^2 + e^{\beta\mu_2}\Xi_d}\right\},$$
$$\Xi_d = 1 + e^{\beta\mu_1}. \tag{15}$$

The free-energy density of the finite-sized spin-$\frac{1}{2}$ Heisenberg diamond chain normalized per spin consequently reads

$$f_{3N} = -k_B T \frac{1}{3N} \ln \mathcal{Z} = \frac{1}{3}\left(J_1 + \frac{J_2}{4}\right) - \frac{1}{3N} k_B T \ln(\lambda_+^N + \lambda_-^N). \tag{16}$$

The simpler expression can be acquired for the free-energy density of the infinite spin-$\frac{1}{2}$ Heisenberg diamond chain, which depends in the thermodynamic limit $N \to \infty$ solely on the larger eigenvalue of the transfer-matrix:

$$f_{\infty} = -k_B T \lim_{N\to\infty} \frac{1}{3N} \ln \mathcal{Z} = \frac{1}{3}\left(J_1 + \frac{J_2}{4}\right) - \frac{1}{3} k_B T \ln \lambda_+. \tag{17}$$

It is noteworthy that the final formulas in Eqs. (16) and (17) for the free-energy density allow a straightforward calculation of the magnetization, susceptibility, entropy, and specific heat for finite and infinite spin-$\frac{1}{2}$ Heisenberg diamond chains, respectively. To verify the reliability of the effective description based on the MD lattice-gas model in Eq. (11), we will compare as-obtained magnetization and specific-heat data with the extensive numerical calculations employing the ED and FTLM implemented within the open-source ALPS [52] and SPINPACK [54,55] software.

First, let us comment on the most interesting results for the highly frustrated spin-$\frac{1}{2}$ Heisenberg diamond chain with $J_2/J_1 > 2$. For illustrative purposes, magnetization curves of the spin-$\frac{1}{2}$ Heisenberg diamond chain are displayed in the left panel of Fig. 7 for the fixed value of the interaction ratio $J_2/J_1 = 2.1$ and four different temperatures. The magnetization data derived from the finite-sized formula in Eq. (16) for the free-energy density of the effective MD model in Eq. (11) are compared in this figure with the full ED data for 18 spins ($N = 6$ unit cells, upper panel) and FTLM results for 30 spins ($N = 10$ unit cells, lower panel) of the spin-$\frac{1}{2}$ Heisenberg diamond chain in Eq. (1). The magnetization curves acquired from the MD model in Eq. (11) perfectly coincide at sufficiently low temperatures $k_B T/J_1 \lesssim 0.2$ with accurate numerical results for the magnetization curves of the spin-$\frac{1}{2}$ Heisenberg diamond chain. Generally, the intermediate $\frac{1}{3}$-plateau resembling the MD ground state gradually shrinks upon increasing of temperature, and the magnetization curve becomes smoother. To gain a more complete understanding, the magnetic-field variations of the specific heat of the spin-$\frac{1}{2}$ Heisenberg diamond chain are depicted in the right panel of Fig. 7 for the same fixed value of the interaction ratio $J_2/J_1 = 2.1$ and three different temperatures. From this figure, the perfect agreement between the specific-heat data stemming from the effective MD model in Eq. (11) and the precise numerical

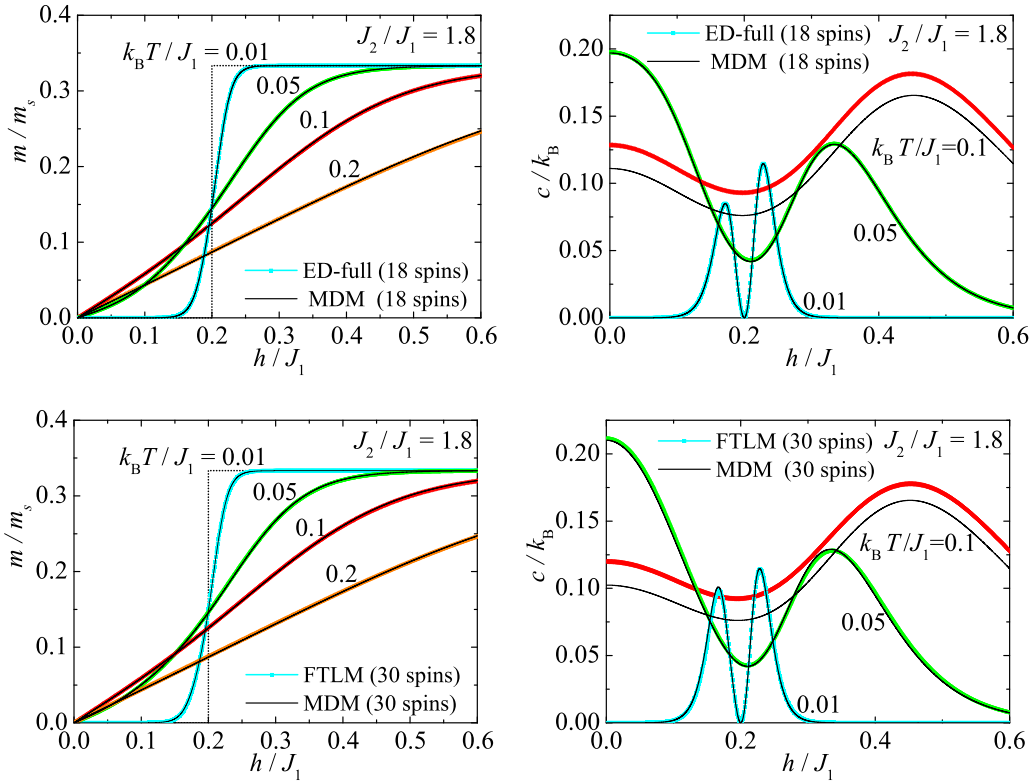

FIG. 8. (Left panel) Magnetization curves of the spin-$\frac{1}{2}$ Heisenberg diamond chain with $J_2/J_1 = 1.8$ obtained from the effective monomer-dimer model (MDM) vs the exact diagonalization (ED) data for 18 spins (upper panel) and the finite-temperature Lanczos method (FTLM) data for 30 spins (lower panel) of the original model in Eq. (1). (Right panel) The same as in the left panel but for the specific heat. Thin black lines show analytical results derived from the effective MDM in Eq. (11), while colored symbols refer to the ED (upper panel) or FTLM (lower panel).

data acquired for the spin-$\frac{1}{2}$ Heisenberg diamond chain in Eq. (1) is limited to much lower temperatures $k_BT/J_1 \lesssim 0.05$, while the discrepancy becomes more pronounced at higher temperatures even if the effective description still at least qualitatively reproduces the most essential features of the accurate numerical data. It should also be pointed out that the magnetization and specific heat of the spin-$\frac{1}{2}$ Heisenberg diamond chain do not show at low enough temperatures almost any finite-sized dependence (confront data for the diamond chain with 18 and 30 spins) because most thermally populated excited states are from the monomeric universality class.

The magnetization process and specific heat are displayed in Fig. 8 for the spin-$\frac{1}{2}$ Heisenberg diamond chain with a relative strength of the interaction constants $J_2/J_1 = 1.8$ promoting a moderately strong spin frustration. Under this condition, the spin-$\frac{1}{2}$ Heisenberg diamond chain exhibits in a low-field region zero and $\frac{1}{3}$ magnetization plateaus, which can be ascribed to the TD and MD ground states, respectively. The magnetization curves extracted from the effective lattice-gas model of hard-core monomers and dimers in Eq. (11) are in excellent agreement with the precise numerical data obtained from the full ED (upper panel) or FTLM (lower panel) up to moderate temperatures $k_BT/J_1 \lesssim 0.2$, see the left panel in Fig. 8. The magnetic-field dependences of the specific heat of the spin-$\frac{1}{2}$ Heisenberg diamond chain are plotted on the right panel of Fig. 8 for the same value of the interaction ratio $J_2/J_1 = 1.8$ and three different temperatures. The specific heat displays in a low-field region a pronounced double-peak dependence, which appears in the vicinity of the field-driven phase transition between the TD and MD ground states emergent at $h/J_1 = 0.2$. Unlike the previous case, the peak heights of the specific heat above and below the relevant field-induced phase transition are not the same due to difference in the relative degeneracy of the TD and MD ground states. It turns out that the low-temperature dependences of the specific heat stemming from the effective MD model in Eq. (11) satisfactorily reproduce the accurate numerical data gained for the spin-$\frac{1}{2}$ Heisenberg diamond chain in Eq. (1) with the help of ED and FTLM only at low enough temperatures $k_BT/J_1 \lesssim 0.05$, whereas there is only qualitative rather than quantitative agreement at higher temperatures $k_BT/J_1 \gtrsim 0.1$. Another interesting observation is that the less frustrated spin-$\frac{1}{2}$ Heisenberg diamond chain with $J_2/J_1 = 1.8$ shows a marked finite-sized effect of the specific heat when both peak heights are at sufficiently low temperatures somewhat higher for the diamond chain with 30 spins than for 18 spins.

To bring insight into the reliability of the developed effective description as well as finite-sized effects, we depict in Fig. 9 temperature variations of the magnetization and specific heat of the spin-$\frac{1}{2}$ Heisenberg diamond chain for the fixed value of the interaction ratio $J_2/J_1 = 1.8$ and two different magnetic fields $h/J_1 = 0.15$ and 0.25 selected slightly below and above the relevant transition field. Temperature dependencies of the magnetization generally exhibit a perfect

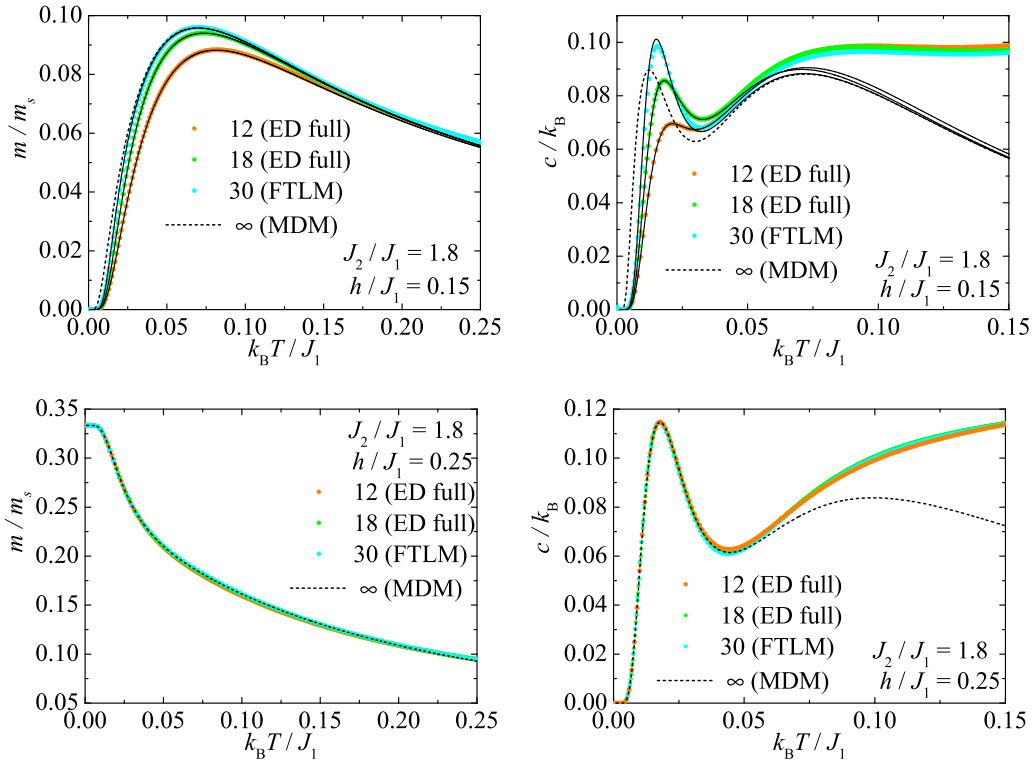

FIG. 9. (Left panel) Temperature dependencies of the magnetization of the spin-$\frac{1}{2}$ Heisenberg diamond chain for $J_2/J_1 = 1.8$ and two different magnetic fields $h/J_1 = 0.15$ (upper panel) and $h/J_1 = 0.25$ (lower panel). (Right panel) The same as in the left panel but for temperature dependencies of the specific heat per spin. Colored symbols display numerical data derived with the help of exact diagonalization (ED) or finite-temperature Lanczos method (FTLM) for the finite-sized diamond-chain model in Eq. (1), while thin black lines (not shown for the lower panel) depict the respective analytical results derived from the effective monomer-dimer model (MDM) in Eq. (11). A black broken line shows a theoretical prediction gained from the effective MDM in Eq. (11) in the thermodynamic limit $N \to \infty$.

agreement between analytical results derived from the effective model (solid lines) and numerical data acquired by ED and FTLM methods (colored symbols) up to moderate temperatures $k_B T/J_1 \lesssim 0.2$. While the magnetization data recorded at higher magnetic fields supporting the MD ground state do not show any marked finite-sized corrections, the magnetization data at lower magnetic fields preferring the TD ground state are subject to a gentle finite-sized effect when the magnetization gradually rises with increasing of the system size. A black broken line displays a valuable theoretical prediction of the effective MD model in Eq. (11) in the thermodynamic limit $N \to \infty$, which is otherwise inaccessible to unperturbed numerical approaches gradually converging to this limit. The same statements hold true also for temperature dependencies of the specific heat with a few small differences. First, the excellent quantitative accordance between the analytical and numerical results can be observed only up to much lower temperature $k_B T/J_1 \lesssim 0.05$, and second, the height of the low-temperature peak of the specific heat does not show the monotonous dependence on a system size at lower magnetic fields when it at first increases and then decreases upon increasing of the number of spins (unit cells). From this perspective, the relevant prediction of the effective MD lattice-gas model in Eq. (11) for the specific heat is especially valuable because it would be otherwise difficult, if not impossible, to estimate the specific-heat data in the thermodynamic limit (black broken line) from a finite-sized analysis of precise numerical methods such as ED or FTLM. The developed localized-magnon theory thus provides a useful alternative to other sophisticated calculation methods, which also allow a precise estimate of thermodynamic properties of diamond spin chain from a full energy spectrum of its smaller fragments [56,57], and that is why the validity of these theories holds up to slightly higher temperatures.

IV. GROUND STATES OF A SPIN-$\frac{1}{2}$ HEISENBERG OCTAHEDRAL CHAIN

Another paradigmatic example to be considered hereafter is the spin-$\frac{1}{2}$ Heisenberg octahedral chain schematically

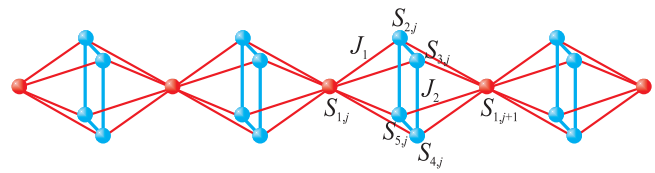

FIG. 10. A schematic illustration of the spin-$\frac{1}{2}$ Heisenberg octahedral chain including notation for the lattice sites and assumed coupling constants.

shown in Fig. 10 and defined via the Hamiltonian:

$$\hat{\mathcal{H}} = \sum_{j=1}^{N}\Big[J_1(\hat{\mathbf{S}}_{1,j}+\hat{\mathbf{S}}_{1,j+1})\cdot(\hat{\mathbf{S}}_{2,j}+\hat{\mathbf{S}}_{3,j}+\hat{\mathbf{S}}_{4,j}+\hat{\mathbf{S}}_{5,j}) + J_2(\hat{\mathbf{S}}_{2,j}\cdot\hat{\mathbf{S}}_{3,j}+\hat{\mathbf{S}}_{3,j}\cdot\hat{\mathbf{S}}_{4,j}+\hat{\mathbf{S}}_{4,j}\cdot\hat{\mathbf{S}}_{5,j}+\hat{\mathbf{S}}_{5,j}\cdot\hat{\mathbf{S}}_{2,j}) - h\sum_{i=1}^{5}\hat{S}^z_{i,j}\Big]. \tag{18}$$

Here, the coupling constant J_2 denotes antiferromagnetic exchange interaction between nearest-neighbor spins from square plaquettes, and the coupling constant J_1 accounts for the nearest-neighbor interaction between monomeric spins and square-plaquette spins. The parameter h stands for the external magnetic field, N is the total number of unit cells, and the periodic boundary condition is assumed $S_{1,N} \equiv S_{1,1}$ for simplicity. A full ground-state phase diagram of the spin-$\frac{1}{2}$ Heisenberg octahedral chain in Eq. (18) was established using the variational technique, localized-magnon approach, Lanczos method, and DMRG calculations in our previous paper [25], to which readers interested in further calculation details are referred to. To make our subsequent discussion self-contained, we will merely quote only the main outcomes of this calculation procedure, which was accomplished in a similar fashion as thoroughly described for the spin-$\frac{1}{2}$ Heisenberg diamond chain in the preceding part.

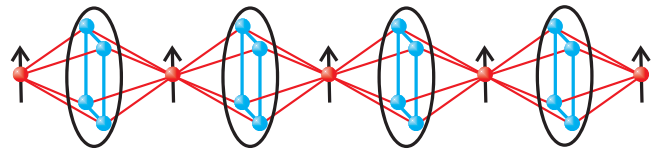

FIG. 11. A schematic illustration of the monomer-tetramer ground state in Eq. (19), which is responsible for occurrence of the intermediate $\frac{1}{5}$ plateau in a zero-temperature magnetization curve. An oval denotes a singlet-tetramer state.

The variational method provides for the spin-$\frac{1}{2}$ Heisenberg octahedral chain in Eq. (18) exact evidence of the monomer-tetramer (MT) ground state in the highly frustrated parameter region $J_2 > 2J_1$ and low enough magnetic fields $h < J_1 + J_2$. The MT ground state is for better illustration schematically drawn in Fig. 11 and can be defined through the eigenvector with the character of a tensor-product state of uncorrelated monomeric spins and singlet tetramers on square plaquettes:

$$|\mathrm{MT}\rangle = \begin{cases} \prod_{j=1}^{N}|S_{1,j}\rangle\otimes\frac{1}{\sqrt{3}}\big[\frac{1}{2}(|\uparrow_{2,j}\uparrow_{3,j}\downarrow_{4,j}\downarrow_{5,j}\rangle + |\uparrow_{2,j}\downarrow_{3,j}\downarrow_{4,j}\uparrow_{5,j}\rangle + |\downarrow_{2,j}\uparrow_{3,j}\uparrow_{4,j}\downarrow_{5,j}\rangle + |\downarrow_{2,j}\downarrow_{3,j}\uparrow_{4,j}\uparrow_{5,j}\rangle) \\ \qquad -|\uparrow_{2,j}\downarrow_{3,j}\uparrow_{4,j}\downarrow_{5,j}\rangle - |\downarrow_{2,j}\uparrow_{3,j}\downarrow_{4,j}\uparrow_{5,j}\rangle\big], \quad h=0, \\ \prod_{j=1}^{N}|\uparrow_{1,j}\rangle\otimes\frac{1}{\sqrt{3}}\big[\frac{1}{2}(|\uparrow_{2,j}\uparrow_{3,j}\downarrow_{4,j}\downarrow_{5,j}\rangle + |\uparrow_{2,j}\downarrow_{3,j}\downarrow_{4,j}\uparrow_{5,j}\rangle + |\downarrow_{2,j}\uparrow_{3,j}\uparrow_{4,j}\downarrow_{5,j}\rangle + |\downarrow_{2,j}\downarrow_{3,j}\uparrow_{4,j}\uparrow_{5,j}\rangle) \\ \qquad -|\uparrow_{2,j}\downarrow_{3,j}\uparrow_{4,j}\downarrow_{5,j}\rangle - |\downarrow_{2,j}\uparrow_{3,j}\downarrow_{4,j}\uparrow_{5,j}\rangle\big], \quad h>0, \end{cases} \tag{19}$$

where $|S_{1,j}\rangle$ denotes any out of two available states $|\uparrow_{1,j}\rangle$ and $|\downarrow_{1,j}\rangle$ of the monomeric spins. It is noteworthy that the monomeric spins are within the MT phase in Eq. (19) completely free to flip at zero magnetic field due to a spin frustration invoked by a singlet-tetramer state, which can be alternatively viewed as a bound two-magnon eigenstate of a square plaquette. Owing to this fact, the monomeric spins become fully polarized by any nonzero external magnetic field, and the MT ground state in Eq. (19) will consequently manifest itself in a zero-temperature magnetization curve as the intermediate $\frac{1}{5}$ plateau.

On the other hand, the localized-magnon theory developed for the spin-$\frac{1}{2}$ Heisenberg octahedral chain furnishes a rigorous proof for the magnon-crystal (MC) ground state, which is schematically shown in Fig. 12 and mathematically given by the eigenvector:

$$|\mathrm{MC}\rangle = \prod_{j=1}^{N}|\uparrow_{1,j}\rangle\otimes\frac{1}{2}(|\downarrow_{2,j}\uparrow_{3,j}\uparrow_{4,j}\uparrow_{5,j}\rangle - |\uparrow_{2,j}\downarrow_{3,j}\uparrow_{4,j}\uparrow_{5,j}\rangle + |\uparrow_{2,j}\uparrow_{3,j}\downarrow_{4,j}\uparrow_{5,j}\rangle - |\uparrow_{2,j}\uparrow_{3,j}\uparrow_{4,j}\downarrow_{5,j}\rangle). \tag{20}$$

The MC phase in Eq. (20) has the character of a tensor-product state of the fully polarized monomeric spins and the bound one-magnon eigenstates, which trap a single magnon within each square plaquette due to the destructive quantum interference ensured by alternating signs of the probability amplitudes. Note furthermore that the MC ground state emerges in the highly frustrated parameter region $J_2 > 2J_1$ and sufficiently high magnetic fields that, however, do not exceed the saturation field $h < h_s = J_1 + 2J_2$.

In the rest of the parameter space $J_2 < 2J_1$, the ground states of the spin-$\frac{1}{2}$ Heisenberg octahedral chain can be found by rewriting the zero-field part of the Hamiltonian in Eq. (18) using the composite spin operator of the square plaquette $\hat{\mathbf{S}}_{c,j} = \hat{\mathbf{S}}_{2,j} + \hat{\mathbf{S}}_{3,j} + \hat{\mathbf{S}}_{4,j} + \hat{\mathbf{S}}_{5,j}$ and two composite operators

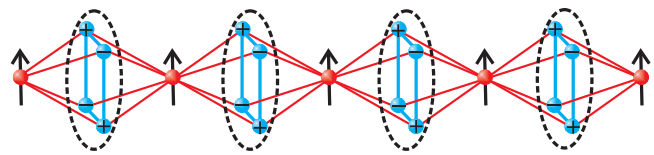

FIG. 12. A schematic illustration of the magnon-crystal ground state in Eq. (20), which is responsible for occurrence of the intermediate $\frac{3}{5}$ plateau in a zero-temperature magnetization curve. An oval denotes a magnon bound to a square plaquette due to a destructive quantum interference caused by alternating signs of the probability amplitudes.

for spin pairs from opposite corners of the square plaquette $\hat{\mathbf{S}}_{24,j} = \hat{\mathbf{S}}_{2,j} + \hat{\mathbf{S}}_{4,j}$ and $\hat{\mathbf{S}}_{35,j} = \hat{\mathbf{S}}_{3,j} + \hat{\mathbf{S}}_{5,j}$:

$$\hat{\mathcal{H}} = J_1 \sum_{j=1}^{N} (\hat{\mathbf{S}}_{1,j} + \hat{\mathbf{S}}_{1,j+1}) \cdot \hat{\mathbf{S}}_{c,j} + \frac{J_2}{2} \sum_{j=1}^{N} \left(\hat{\mathbf{S}}_{c,j}^2 - \hat{\mathbf{S}}_{24,j}^2 - \hat{\mathbf{S}}_{35,j}^2 \right). \tag{21}$$

The composite spin operators $\hat{\mathbf{S}}_{c,j}$, $\hat{\mathbf{S}}_{24,j}$, and $\hat{\mathbf{S}}_{35,j}$ commute with the Hamiltonian in Eq. (21), and thus, they correspond to conserved quantities with well-defined spin quantum numbers $S_{c,j} = 0$, 1, or 2; $S_{24,j} = 0$ or 1; and $S_{35,j} = 0$ or 1. The spin-$\frac{1}{2}$ Heisenberg octahedral chain becomes equivalent to the effective mixed spin-($\frac{1}{2}$, S_c) Heisenberg chains (see Fig. 3) whose eigenenergies are only trivially shifted due to the second term of the Hamiltonian in Eq. (21) depending on the quantum spin numbers $S_{c,j}$, $S_{24,j}$, and $S_{35,j}$.

The lowest-energy eigenstates of the effective mixed spin-($\frac{1}{2}$, S_c) Heisenberg chains were previously obtained by extensive DMRG simulations [25] implemented within the open-source ALPS software [52]. If the four spins forming a square plaquette are in the singlet-tetramer state, i.e., the composite spin of a square plaquette becomes zero $S_{c,j} = 0$, then the spin-$\frac{1}{2}$ Heisenberg octahedral chain is broken into smaller fragments due to a lack of spin-spin correlations across this square plaquette. A few exact fragmented ground states can be found using this procedure. In this way, one recovers, for instance, the MT ground state in Eq. (19) by considering $\forall j \; S_{c,j} = 0$ and the MC ground state in Eq. (20) when assuming $\forall j \; S_{c,j} = 1$. In addition, the regular alternation of the composite spin values $S_{c,2j-1} = 1$ and $S_{c,2j} = 0$ within the effective mixed spin-($\frac{1}{2}$,1,$\frac{1}{2}$,0) Heisenberg chain results in the singlet TH phase given by the eigenvector:

$$\begin{aligned}
|\mathrm{TH}\rangle = \prod_{j=1}^{N/2} \frac{1}{\sqrt{3}} \Big[& |\uparrow_{2,2j-1}\downarrow_{3,2j-1}\uparrow_{4,2j-1}\downarrow_{5,2j-1}\rangle + |\downarrow_{2,2j-1}\uparrow_{3,2j-1}\downarrow_{4,2j-1}\uparrow_{5,2j-1}\rangle - \frac{1}{2}|\uparrow_{2,2j-1}\uparrow_{3,2j-1}\downarrow_{4,2j-1}\downarrow_{5,2j-1}\rangle \\
& - \frac{1}{2}(|\uparrow_{2,2j-1}\downarrow_{3,2j-1}\downarrow_{4,2j-1}\uparrow_{5,2j-1}\rangle + |\downarrow_{2,2j-1}\uparrow_{3,2j-1}\uparrow_{4,2j-1}\downarrow_{5,2j-1}\rangle + |\downarrow_{2,2j-1}\downarrow_{3,2j-1}\uparrow_{4,2j-1}\uparrow_{5,2j-1}\rangle) \Big] \\
& \times \otimes \frac{1}{\sqrt{12}} (|\uparrow_{1,2j}\uparrow_{2,2j}\downarrow_{3,2j}\uparrow_{4,2j}\downarrow_{5,2j}\downarrow_{1,2j+1}\rangle + |\downarrow_{1,2j}\uparrow_{2,2j}\downarrow_{3,2j}\uparrow_{4,2j}\downarrow_{5,2j}\uparrow_{1,2j+1}\rangle + |\uparrow_{1,2j}\downarrow_{2,2j}\uparrow_{3,2j}\downarrow_{4,2j}\downarrow_{5,2j}\uparrow_{1,2j+1}\rangle \\
& + |\uparrow_{1,2j}\downarrow_{2,2j}\downarrow_{3,2j}\downarrow_{4,2j}\uparrow_{5,2j}\uparrow_{1,2j+1}\rangle + |\downarrow_{1,2j}\uparrow_{2,2j}\uparrow_{3,2j}\downarrow_{4,2j}\uparrow_{5,2j}\downarrow_{1,2j+1}\rangle + |\downarrow_{1,2j}\downarrow_{2,2j}\uparrow_{3,2j}\uparrow_{4,2j}\uparrow_{5,2j}\downarrow_{1,2j+1}\rangle \\
& - |\uparrow_{1,2j}\downarrow_{2,2j}\uparrow_{3,2j}\downarrow_{4,2j}\uparrow_{5,2j}\downarrow_{1,2j+1}\rangle - |\downarrow_{1,2j}\downarrow_{2,2j}\uparrow_{3,2j}\downarrow_{4,2j}\uparrow_{5,2j}\uparrow_{1,2j+1}\rangle - |\uparrow_{1,2j}\uparrow_{2,2j}\downarrow_{3,2j}\downarrow_{4,2j}\downarrow_{5,2j}\uparrow_{1,2j+1}\rangle \\
& - |\uparrow_{1,2j}\downarrow_{2,2j}\downarrow_{3,2j}\uparrow_{4,2j}\downarrow_{5,2j}\uparrow_{1,2j+1}\rangle - |\downarrow_{1,2j}\uparrow_{2,2j}\uparrow_{3,2j}\uparrow_{4,2j}\downarrow_{5,2j}\downarrow_{1,2j+1}\rangle - |\downarrow_{1,2j}\uparrow_{2,2j}\downarrow_{3,2j}\uparrow_{4,2j}\uparrow_{5,2j}\downarrow_{1,2j+1}\rangle).
\end{aligned} \tag{22}$$

The singlet TH phase schematically shown in Fig. 13 is in fact twofold degenerate because another linearly independent eigenstate with the same energy can be obtained from the eigenvector in Eq. (22) by interchanging singlet-tetramer and singlet-hexamer states on odd and even unit cells. The TH phase emerges only if the interaction ratio is from the interval $0.91 < J_2/J_1 < 2.0$ and the magnetic field is sufficiently small $h/J_1 < 0.55$, whereby the highest possible field value for existence of the TH ground state is achieved for $J_2/J_1 \approx 1.45$, see Fig. 14.

As can be seen in Fig. 14, the overall ground-state phase diagram of the spin-$\frac{1}{2}$ Heisenberg octahedral chain reveals a great diversity of remarkable quantum ground states including two ferrimagnetic Lieb-Mattis phases originating from the mixed spin-($\frac{1}{2}$, 1) and mixed spin-($\frac{1}{2}$, 2) Heisenberg chains, respectively, two quantum spin-liquid phases derived from

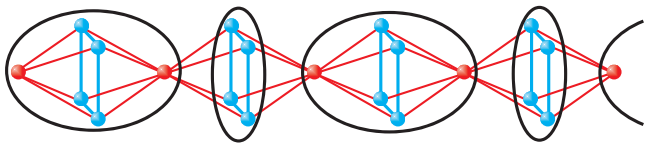

FIG. 13. A schematic illustration of the singlet tetramer-hexamer phase in Eq. (22), which leads to occurrence of zero plateau in a zero-temperature magnetization curve. Small and large ovals correspond to the singlet-tetramer and singlet-hexamer state, respectively.

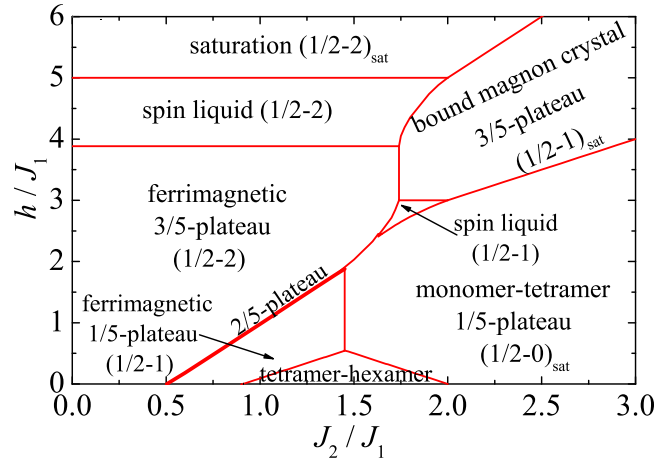

FIG. 14. The ground-state phase diagram of the spin-$\frac{1}{2}$ Heisenberg octahedral chain in the $J_2/J_1 - h/J_1$ plane.

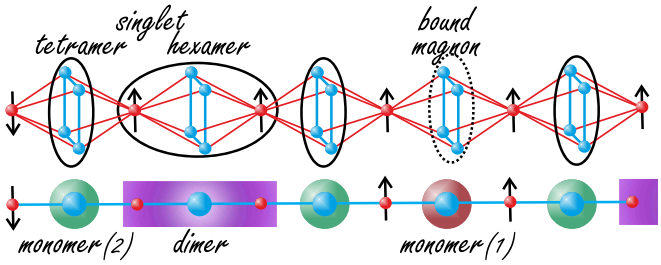

FIG. 15. A schematic illustration of one paradigmatic eigenstate of the spin-$\frac{1}{2}$ Heisenberg octahedral chain and its equivalent representation within the three-component lattice-gas model of hard-core monomers and dimers. Small red spheres of the auxiliary lattice correspond to the monomeric spins $S_{1,j}$, while large blue spheres of the auxiliary lattice correspond to the composite spins $S_{c,j}$ assigned to the square plaquettes occupied by one of two monomeric particles or a dimeric particle.

the same couple of mixed-spin Heisenberg chains closing an energy gap above the Lieb-Mattis ferrimagnetic phases, the gapful ferrimagnetic phase with a translationally broken symmetry, the fully polarized ferromagnetic phase, and three additional fragmented ground states denoted as the MT phase [see Eq. (19) and Fig. 11], the bound MC phase [see Eq. (20) and Fig. 12)], and the singlet TH phase [see Eq. (22) and Fig. 13].

V. HEISENBERG OCTAHEDRAL CHAIN AS MD PROBLEM

In the following part, we investigate in detail low-temperature magnetization curves and thermodynamics of the spin-$\frac{1}{2}$ Heisenberg octahedral chain as extracted from the anticipated one-dimensional lattice-gas model of hard-core monomers and dimers. Recently, we have convincingly evidenced that the simpler version of the localized-magnon theory based on an effective one-dimensional lattice gas including two types of hard-core monomeric particles ascribed to bound one- and two-magnon eigenstates of square plaquettes provides within the highly frustrated parameter region $J_2/J_1 > 2$ a proper description of low-temperature magnetization curves and thermodynamics of the spin-$\frac{1}{2}$ Heisenberg octahedral chain from zero up to the saturation field [25,26]. The main goal of this paper is to extend the validity of the localized-magnon theory to a less frustrated parameter space additionally involving the singlet TH phase in Eq. (22). The idea and calculation procedure is quite similar as previously elucidated for the spin-$\frac{1}{2}$ Heisenberg diamond chain.

The low-energy physics of the spin-$\frac{1}{2}$ Heisenberg octahedral chain are effectively described by the lattice-gas model of hard-core monomers and dimers defined on auxiliary one-dimensional lattice, which may include the monomeric particle assigned to the singlet-tetramer (i.e., bound two-magnon) eigenstate of a square plaquette:

$$|m\rangle_j = \frac{1}{\sqrt{3}}\Big[|\uparrow_{2,j}\downarrow_{3,j}\uparrow_{4,j}\downarrow_{5,j}\rangle + |\downarrow_{2,j}\uparrow_{3,j}\downarrow_{4,j}\uparrow_{5,j}\rangle - \frac{1}{2}(|\uparrow_{2,j}\uparrow_{3,j}\downarrow_{4,j}\downarrow_{5,j}\rangle + |\uparrow_{2,j}\downarrow_{3,j}\downarrow_{4,j}\uparrow_{5,j}\rangle) - \frac{1}{2}(|\downarrow_{2,j}\uparrow_{3,j}\uparrow_{4,j}\downarrow_{5,j}\rangle + |\downarrow_{2,j}\downarrow_{3,j}\uparrow_{4,j}\uparrow_{5,j}\rangle)\Big], \tag{23}$$

the monomeric particle assigned to the bound one-magnon eigenstate of a square plaquette:

$$|n\rangle_j = \tfrac{1}{2}(|\downarrow_{2,j}\uparrow_{3,j}\uparrow_{4,j}\uparrow_{5,j}\rangle - |\uparrow_{2,j}\downarrow_{3,j}\uparrow_{4,j}\uparrow_{5,j}\rangle + |\uparrow_{2,j}\uparrow_{3,j}\downarrow_{4,j}\uparrow_{5,j}\rangle - |\uparrow_{2,j}\uparrow_{3,j}\uparrow_{4,j}\downarrow_{5,j}\rangle), \tag{24}$$

as well as, the dimeric particle assigned to the singlet-hexamer state of a octahedron (six-spin) cluster being a cornerstone of the TH ground states in Eq. (22)

$$|d\rangle_j = \frac{1}{\sqrt{12}}(|\uparrow_{1,2j}\uparrow_{2,2j}\downarrow_{3,2j}\uparrow_{4,2j}\downarrow_{5,2j}\downarrow_{1,2j+1}\rangle + |\downarrow_{1,2j}\uparrow_{2,2j}\downarrow_{3,2j}\uparrow_{4,2j}\downarrow_{5,2j}\uparrow_{1,2j+1}\rangle + |\uparrow_{1,2j}\downarrow_{2,2j}\uparrow_{3,2j}\downarrow_{4,2j}\downarrow_{5,2j}\uparrow_{1,2j+1}\rangle + |\uparrow_{1,2j}\downarrow_{2,2j}\downarrow_{3,2j}\downarrow_{4,2j}\uparrow_{5,2j}\uparrow_{1,2j+1}\rangle + |\downarrow_{1,2j}\uparrow_{2,2j}\uparrow_{3,2j}\downarrow_{4,2j}\uparrow_{5,2j}\downarrow_{1,2j+1}\rangle + |\downarrow_{1,2j}\downarrow_{2,2j}\uparrow_{3,2j}\uparrow_{4,2j}\uparrow_{5,2j}\downarrow_{1,2j+1}\rangle - |\uparrow_{1,2j}\downarrow_{2,2j}\uparrow_{3,2j}\downarrow_{4,2j}\uparrow_{5,2j}\downarrow_{1,2j+1}\rangle - |\downarrow_{1,2j}\downarrow_{2,2j}\uparrow_{3,2j}\downarrow_{4,2j}\uparrow_{5,2j}\uparrow_{1,2j+1}\rangle - |\uparrow_{1,2j}\uparrow_{2,2j}\downarrow_{3,2j}\downarrow_{4,2j}\downarrow_{5,2j}\uparrow_{1,2j+1}\rangle - |\uparrow_{1,2j}\downarrow_{2,2j}\downarrow_{3,2j}\uparrow_{4,2j}\downarrow_{5,2j}\uparrow_{1,2j+1}\rangle - |\downarrow_{1,2j}\uparrow_{2,2j}\uparrow_{3,2j}\uparrow_{4,2j}\downarrow_{5,2j}\downarrow_{1,2j+1}\rangle - |\downarrow_{1,2j}\uparrow_{2,2j}\downarrow_{3,2j}\uparrow_{4,2j}\uparrow_{5,2j}\downarrow_{1,2j+1}\rangle). \tag{25}$$

One paradigmatic example of the feasible eigenstate of the spin-$\frac{1}{2}$ Heisenberg octahedral chain and its equivalent representation within the designed MD lattice-gas model is illustrated in Fig. 15. Small red spheres of the auxiliary lattice correspond to lattice sites of the monomeric spins $S_{1,j}$, and large blue spheres of the auxiliary lattice correspond to lattice positions of the composite spins $S_{c,j} = S_{2,j} + S_{3,j} + S_{4,j} + S_{5,j}$ of the square plaquettes, which are available to the fully polarized ferromagnetic state acting as a reference vacuum state, the singlet-tetramer state in Eq. (23) represented by the monomeric particle shown as a large green sphere, the bound one-magnon state in Eq. (24) represented by the monomeric particle depicted as a large brown sphere, and the singlet-hexamer state in Eq. (25) represented by the dimeric particle displayed as a large violet rectangle involving two neighboring monomeric spins $S_{1,j}$ and $S_{1,j+1}$ as well. In what follows, the energy of the square plaquettes is determined relative to the fully polarized ferromagnetic state serving as a reference state, and consequently, one should assign the chemical potential $\mu_1^{(2)} = 2J_1 + 3J_2 - 2h$ to the monomeric particles assigned to the bound two-magnon state in Eq. (23), the chemical potential $\mu_1^{(1)} = J_1 + 2J_2 - h$ to the monomeric particles connected to the bound one-magnon state in Eq. (24), and the chemical potential $\mu_2 = 3J_1 - h$ to the dimeric particles ascribed to the singlet-hexamer state in Eq. (25). The effective MD lattice-gas model can then be defined through

the Hamiltonian:

$$\mathcal{H} = E^0_{\rm FM} - h\sum_{j=1}^{N}\left[2 + S^z_{1,j}(1-d_{j-1})(1-d_j)\right] - \mu_1^{(2)}\sum_{j=1}^{N} m_j - \mu_1^{(1)}\sum_{j=1}^{N} n_j - \mu_2\sum_{j=1}^{N} d_j, \tag{26}$$

where $E^0_{\rm FM}=2NJ_1+NJ_2$ is zero-field energy of the fully polarized ferromagnetic state, the second term is the Zeeman's term, and $m_j=0, 1$, $n_j=0, 1$, and $d_j=0, 1$ label occupation numbers for three kinds of particles additionally obeying hard-core constraint since each square plaquette of the spin-$\frac{1}{2}$ Heisenberg octahedral chain may be at most in one out of three considered eigenstates in Eqs. (23)–(25). The partition function of the effective MD lattice-gas model given by the Hamiltonian in Eq. (26) can be calculated from the formula:

$$\mathcal{Z} = \exp\left(-\beta E^0_{\rm FM}\right)\sum_{\{S^z_{1,j}\}}\sum_{\{m_j\}}\sum_{\{n_j\}}\sum_{\{d_j\}}\prod_{j=1}^{N}\frac{1}{4^{d_j}}(1-d_{j-1}d_j)(1-m_jd_j)(1-n_jd_j)(1-m_jn_j)\exp\left\{\beta\left[\mu_1^{(2)}m_j+\mu_1^{(1)}n_j+\mu_2 d_j\right]\right\} \times \exp\left[\beta h S^z_{1,j}(1-d_{j-1})(1-d_j)\right], \tag{27}$$

which already includes the factor $(1-d_{j-1}d_j)(1-m_jd_j)(1-n_jd_j)(1-m_jn_j)$, ensuring a hard-core rule that prevents overlap and/or double occupancy of auxiliary lattice sites by the monomeric and dimeric particles. The other factor $\frac{1}{4^{d_j}}$ entering into the partition function in Eq. (27) is the correction term for the singlet-hexamer state in Eq. (25), which avoids fourfold counting of this eigenstate when performing the summation over spin states of two monomeric spins $S_{1,j}$ and $S_{1,j+1}$. As in Sec. III, we note that the partition function above contains the forbidden configurations when the singlet-plaquette state is followed by the fully polarized or bound one-magnon state on the neighboring dimer. However, since the energies of these two configurations are rather high, they have no effect on the low-temperature thermodynamic properties studied here. After performing the summations $\sum_{\{S^z_{1,j}\}}$, $\sum_{\{m_j\}}$, and $\sum_{\{n_j\}}$ over sets of the monomeric spins and monomeric hard-core particles, one gets the expression behind the product symbol depending exclusively on the occupation numbers of the dimeric particles:

$$T(d_j,d_{j+1}) = \frac{1}{4^{d_j}}(1-d_{j-1}d_j)\cosh\left[\frac{\beta h}{2}(1-d_{j-1})(1-d_j)\right]2\exp\left(2\beta h+\beta\mu_2 d_j\right)\left(1+(1-d_j)\left\{\exp\left[\beta\mu_1^{(1)}\right]+\exp\left[\beta\mu_1^{(2)}\right]\right\}\right), \tag{28}$$

which can be repeatedly identified with the transfer matrix [cf. Eq. (13)], further simplifying the exact calculation of the partition function according to the standard procedure:

$$\mathcal{Z} = \exp\left(-\beta E^0_{\rm FM}\right)\sum_{\{d_j\}}\prod_{j=1}^{N} T(d_{j-1},d_j) = \exp\left(-\beta E^0_{\rm FM}\right){\rm Tr}T^N = \exp\left(-\beta E^0_{\rm FM}\right)(\lambda_+^N+\lambda_-^N). \tag{29}$$

The final formula for the partition function in Eq. (29) is expressed in terms of eigenvalues $\lambda_\pm$ of a two-by-two transfer matrix in Eq. (28) easily accessible through a direct diagonalization:

$$\lambda_\pm = e^{2\beta h}\left\{\cosh\left(\frac{\beta h}{2}\right)\Xi_o \pm \sqrt{\left[\cosh\left(\frac{\beta h}{2}\right)\Xi_o\right]^2+\exp\left(\beta\mu_2\right)\Xi_o}\right\}, \quad \Xi_o = 1+\exp\left[\beta\mu_1^{(1)}\right]+\exp\left[\beta\mu_1^{(2)}\right], \tag{30}$$

which have quite analogous form to the one previously reported for the spin-$\frac{1}{2}$ Heisenberg diamond chain, cf. Eq. (15). The free-energy density of the finite-sized spin-$\frac{1}{2}$ Heisenberg octahedral chain normalized per spin takes the following form:

$$f_{5N} = -k_{\rm B}T\frac{1}{5N}\ln\mathcal{Z} = \frac{1}{5}(2J_1+J_2) - \frac{1}{5N}k_{\rm B}T\ln(\lambda_+^N+\lambda_-^N), \tag{31}$$

which can be further simplified in the thermodynamic limit $N\to\infty$ when the free-energy density of the infinite spin-$\frac{1}{2}$ Heisenberg octahedral chain per spin is solely expressed in terms of the larger transfer-matrix eigenvalue:

$$f_\infty = -k_{\rm B}T\lim_{N\to\infty}\frac{1}{5N}\ln\mathcal{Z} = \frac{1}{5}(2J_1+J_2) - \frac{1}{5}k_{\rm B}T\ln\lambda_+. \tag{32}$$

The final formulas in Eqs. (31) and (32) for the free-energy density may be subsequently employed for a straightforward calculation of the magnetization, susceptibility, entropy, and specific heat of finite and infinite spin-$\frac{1}{2}$ Heisenberg octahedral chains, respectively. The correctness of the effective description based on the MD lattice-gas model in Eq. (26) is exemplified through a comparison of the as-obtained magnetization and specific-heat data with extensive numerical calculations employing the full ED and FTLM implemented within the open-source ALPS [52] and SPINPACK [54,55] software.

First, the magnetization and specific heat of the spin-$\frac{1}{2}$ Heisenberg octahedral chain are plotted in Fig. 16 as a function of the magnetic field for the interaction ratio $J_2/J_1 = 2.1$. The spin-$\frac{1}{2}$ Heisenberg octahedral chain apparently exhibits two intermediate magnetization plateaus at $\frac{1}{5}$ and $\frac{3}{5}$ of the

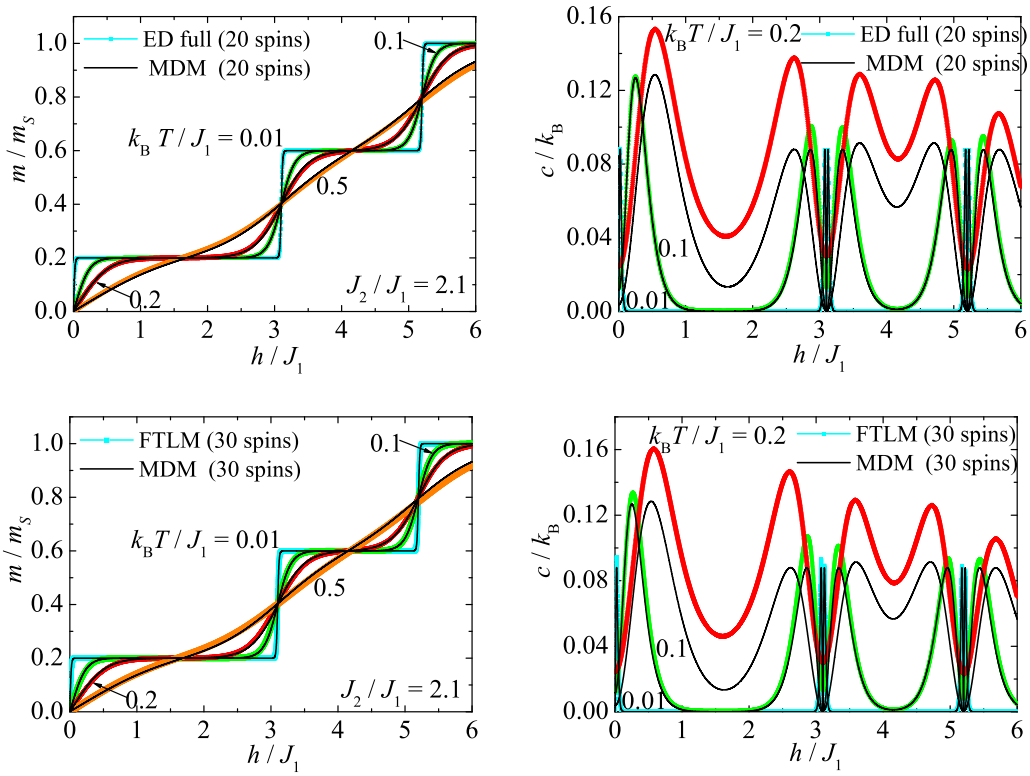

FIG. 16. (Left panel) Magnetization curves of the spin-$\frac{1}{2}$ Heisenberg octahedral chain with $J_2/J_1 = 2.1$ obtained from the effective monomer-dimer model (MDM) vs the exact diagonalization (ED) data for 20 spins (upper panel) and the finite-temperature Lanczos method (FTLM) data for 30 spins (lower panel) of the original model in Eq. (18). (Right panel) The same as in the left panel but for the specific heat. Thin black lines show analytical results derived from the effective MDM in Eq. (26), while colored symbols refer to the ED (upper panel) or FTLM (lower panel) data.

saturation magnetization, which can be attributed to the MT and MC ground states unambiguously given by the eigenvectors in Eqs. (19) and (20), respectively. It directly follows from Fig. 16 that the magnetization curves descended from the effective MD lattice-gas model are in perfect agreement with the full ED data for 20 spins and FTLM data for 30 spins up to moderate temperature $k_B T/J_1 \approx 0.5$. The perfect concordance is a direct consequence of a proper counting of localized many-magnon eigenstates (including among others two realized MT and MC ground states), which form a low-lying part of the energy spectrum being most relevant at low enough temperatures. On the other hand, the magnetic-field variations of the specific heat display more pronounced discrepancies already at much lower temperatures $k_B T/J_1 \gtrsim 0.1$, above which collective quantum states not accounted in the anticipated MD lattice-gas model are sufficiently thermally populated to cause conspicuous uprise with respect to the specific-heat value originating entirely from the many-magnon eigenstates. Despite this shortcoming, the MD lattice-gas model at least qualitatively reproduces a double-peak feature of the specific heat observable in the vicinity of all field-driven phase transitions at low and moderate temperatures.

Last but not least, the low-field part of the magnetization curves of the spin-$\frac{1}{2}$ Heisenberg octahedral chain is depicted in the left panel of Fig. 17 for the less frustrated parameter region $J_2/J_1 = 1.8$, where the investigated quantum spin chain undergoes a field-driven phase transition from the TH state in Eq. (22) to the MT state in Eq. (19). It can be understood from Fig. 17 that the effective MD model in Eq. (26) not only properly reproduces the zero magnetization plateau attributable to the TH phase in Eq. (22), but it also features the field-driven phase transition to the $\frac{1}{5}$ plateau pertinent to the MT phase in Eq. (19) and a gradual smoothing of the magnetization curves achieved upon raising the temperature. The numerical ED and FTLM data indeed bear evidence to the legitimacy of this effective description up to moderate temperature $k_B T/J_1 \approx 0.2$, which is, however, nearly half of the temperature set as the upper bound for a reasonable description of the magnetization curves in the highly frustrated parameter space $J_2/J_1 > 2$. Furthermore, the specific heat of the spin-$\frac{1}{2}$ Heisenberg octahedral chain with the interaction ratio $J_2/J_1 = 1.8$ also displays an intriguing double-peak dependence on the magnetic field as exemplified in the right panel of Fig. 17. The validity of the effective description of the specific heat of the spin-$\frac{1}{2}$ Heisenberg octahedral chain is again limited to relatively low temperatures $k_B T/J_1 \lesssim 0.1$, above which the effective MD model fails to reproduce the precise numerical ED and FTLM data at a quantitative level and provides qualitative insight only. Nevertheless, it should be mentioned that the difference in the height of two round maxima of the specific heat around the field-induced phase transition can be simply interpreted in terms of the effective MD lattice-gas model in Eq. (26). The height of the specific-heat maximum is lower below the respective field-

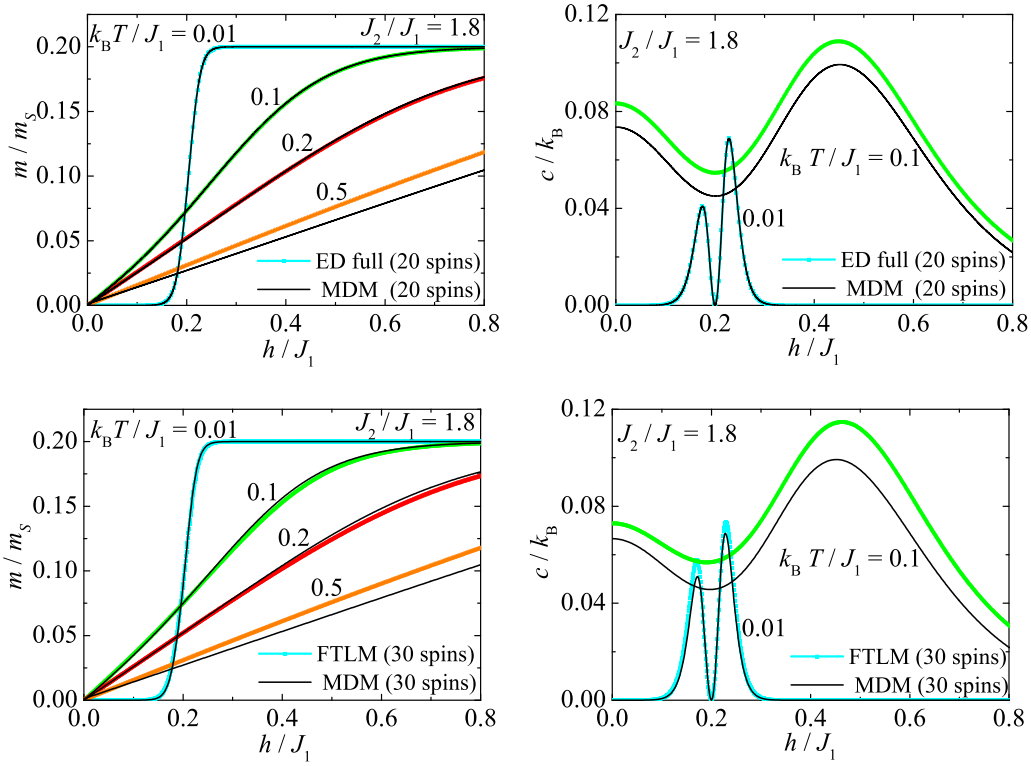

FIG. 17. (Left panel) Magnetization curves of the spin-$\frac{1}{2}$ Heisenberg octahedral chain with $J_2/J_1 = 1.8$ obtained from the effective monomer-dimer model (MDM) vs the exact diagonalization (ED) data for 20 spins (upper panel) and the finite-temperature Lanczos method (FTLM) data for 30 spins (lower panel) of the original model in Eq. (18). (Right panel) The same as in the left panel but for the specific heat. Thin black lines show analytical results derived from the effective MDM in Eq. (26), while colored symbols refer to the ED (upper panel) or FTLM (lower panel) data.

driven phase transition because thermal excitations from the twofold degenerate TH state in Eq. (22) are less intense than the ones from the nondegenerate MT state in Eq. (19).

Our discussion ends with a detailed analysis of temperature variations of the magnetization and specific heat of the spin-$\frac{1}{2}$ Heisenberg octahedral chain, which are plotted in Fig. 18 for the fixed value of the interaction ratio $J_2/J_1 = 1.8$ and two different magnetic fields $h/J_1 = 0.15$ and 0.25. From this figure, there is a reasonable quantitative accordance between analytical results derived for temperature dependencies of the magnetization from the effective MD lattice-gas model (solid lines) and numerical data calculated for the original model by employing ED and FTLM methods (colored symbols), which persists up to moderate temperatures $k_B T/J_1 \lesssim 0.2$. Any obvious traces of finite-sized corrections are repeatedly missing in the magnetization data calculated at higher magnetic fields promoting the MT ground state, whereas small finite-sized effects can be detected in the magnetization data at lower magnetic fields being responsible for the TH ground state for which the magnetization gradually rises with increasing of the system size. A theoretical prediction for the magnetization in the thermodynamic limit $N \to \infty$ as obtained from the effective MD model in Eq. (26) is also displayed in Fig. 18 (left panel) by a black broken line. Next, temperature variations of the specific heat are depicted in Fig. 18 (right panel). As far as the quantitative agreement between the analytical and numerical results is concerned, the specific heat is well captured by the effective MD model in Eq. (11) only at relatively low temperatures $k_B T/J_1 \lesssim 0.05$ regardless of a strength of the magnetic field. The specific heat at higher magnetic fields is repeatedly free of any finite-sized corrections, which become relevant at lower magnetic fields where a nontrivial shift of the height and position of the low-temperature maximum can be observed. It is worth mentioning that a small quantitative discrepancy observable around the low-temperature peak between analytical results derived from the effective MD lattice-gas model in Eq. (11) and numerical data obtained for the octahedral chain with 30 spins within FTLM gradually diminish upon increasing the number of random vectors.

VI. CONCLUSIONS

This paper is devoted to magnetic properties of the spin-$\frac{1}{2}$ Heisenberg diamond and octahedral chains, which are inferred from one-dimensional lattice-gas models of hard-core monomers and dimers deduced by means of the modified localized-magnon theory. An eligibility of the MD lattice-gas models for elucidation of low-temperature magnetization curves and thermodynamic quantities of the spin-$\frac{1}{2}$ Heisenberg diamond and octahedral chains was decisively confirmed by state-of-the-art numerical calculations based on the ED and FTLM. In addition to this, the ground-state phase diagrams of the spin-$\frac{1}{2}$ Heisenberg diamond and octahedral chains were established by making use of exact and DMRG calculations.

It has been evidenced that the anticipated MD lattice-gas model provides a proper description of the spin-$\frac{1}{2}$ Heisenberg

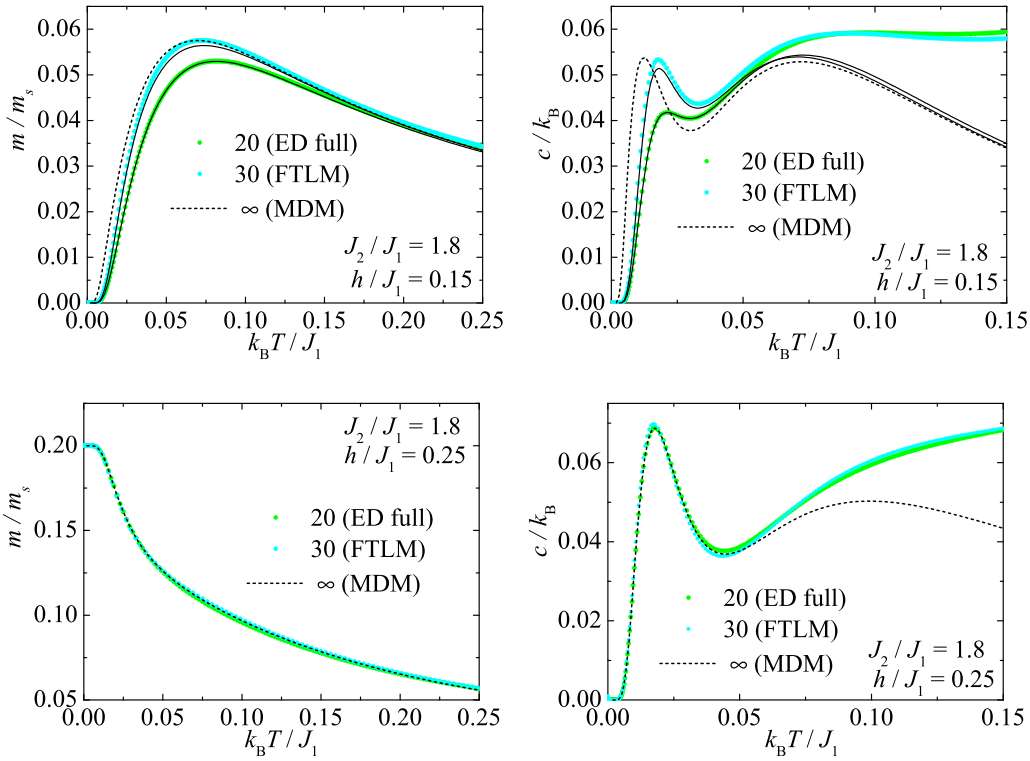

FIG. 18. (Left panel) Temperature dependencies of the magnetization of the spin-$\frac{1}{2}$ Heisenberg octahedral chain for $J_2/J_1 = 1.8$ and two different magnetic fields $h/J_1 = 0.15$ (upper panel) and $h/J_1 = 0.25$ (lower panel). (Right panel) The same as in the left panel but for temperature dependencies of the specific heat per spin. Colored symbols display numerical data derived with the help of exact diagonalization (ED) or finite-temperature Lanczos method (FTLM) for the finite-sized octahedral-chain model in Eq. (18), while thin black lines (not shown for the lower panel) depict the respective analytical results derived from the effective monomer-dimer model (MDM) in Eq. (26). A black broken line shows a theoretical prediction gained from the effective MDM in Eq. (26) in the thermodynamic limit $N \to \infty$.

diamond chain when it is driven by the interaction parameters either to the singlet TD phase, the MD phase, or the saturated ferromagnetic phase. Similarly, the MD lattice-gas model captures low-temperature features of the spin-$\frac{1}{2}$ Heisenberg octahedral chain provided that it is driven to the singlet TH phase, the MT phase, the bound MC phase, or the saturated ferromagnetic phase. The developed localized-magnon theory also brings insight into a remarkable behavior of the specific heat, which shows a marked minimum at magnetic fields inherent to discontinuous field-driven phase transitions that is surrounded by two generally asymmetric round peaks originating from vigorous thermal excitations to low-lying localized many-magnon eigenstates. Note furthermore that the previous localized-magnon theories [23,25] valid only in a highly frustrated parameter region $J_2/J_1 > 2$ can be recovered from Eqs. (15) and (30) after neglecting the second term under the square root in the limit of sufficiently low temperatures and positive magnetic fields.

Let us conclude our study by presenting a few future outlooks. We are convinced that the proposed calculation scheme has opened the route to a low-temperature magnetic behavior of several frustrated Heisenberg spin models, which have at least two tensor-product ground states with a magnetic unit spread over one and two unit cells, respectively. The mixed spin-$(1,\frac{1}{2})$ Heisenberg octahedral chain affords a suitable platform for implementation of the lattice-gas model of hard-core monomers and dimers, which would extend a legitimacy of the previous calculations based on the lattice-gas model of hard-core monomers [27]. Note furthermore that the suggested calculation procedure is also compatible with recent extension enabling a straightforward computation of entanglement measures [28]. Most importantly, the low-temperature physics of two-dimensional frustrated Heisenberg spin models with two tensor-product ground states, which have magnetic unit spread over one and two unit cells, would be captured by a two-dimensional lattice-gas model of hard-core monomers and dimers. Finally, the spin-$\frac{1}{2}$ Heisenberg orthogonal-dimer chain [58] and the mixed-spin Heisenberg diamond chain [59] with an infinite series of fragmented quantum ground states provide another intriguing platform for further extension of the present approach, which would, however, require consideration of one-dimensional lattice-gas models of hard-core monomers, dimers, trimers, tetramers, etc.

ACKNOWLEDGMENTS

J.Str. and K.K. acknowledge kind hospitality during summer 2021 at the Max-Planck-Institut für Physik Komplexer Systeme in Dresden, where a part of this work was completed. J.Str. and K.K. acknowledge financial support provided by the grant of the Ministry of Education, Science, Research and Sport of the Slovak Republic under Contract No. VEGA 1/0105/20 and by the grant of the Slovak Research and Development Agency under the Contracts No. APVV-16-0186

and No. APVV-20-0150. J.R. and J. Sch. acknowledge a Deutsche Forschungsgemeinschaft grants DFG RI 615/25-1 and SCHN 615/28-1.

APPENDIX: ANALYSIS OF THE FRAGMENTED GROUND STATES OF THE DIAMOND CHAIN

It is evident that the singlet state on a dimer breaks the chain into noninteracting parts, leading to the fragmented ground state. This aspect has been considered accurately for the diamond chain in zero field [29]. We will follow a similar argument here. Let us consider the energy of the fragment of the diamond chain where n subsequent dimers are in spin-1 state surrounded by the singlet dimers. Then the ground-state energy per unit cell of such a $(n+1)$ periodic state can be presented as

$$e_n(h) = \tilde{e}_n(h) + \frac{n}{n+1}J_2 - \frac{3}{4}J_2, \tag{A1}$$

where $\tilde{e}_n(h)$ is the minimal energy of the corresponding mixed spin-$(\frac{1}{2}, 1)$ chain with $(n+1)$ spins $\frac{1}{2}$ alternating by n spins 1. The case $n = 0$ with the energy $e_0(h) = \frac{h}{2} - \frac{3}{4}J_2$ corresponds to the MD phase in Eq. (2), while $n = 1$ matches the TD phase composed of alternating singlet tetramers and dimers with the energy:

$$e_1(h) = -J_1 + \tfrac{1}{2}J_2 - \tfrac{3}{4}J_2. \tag{A2}$$

For the states of longer periods, one needs to perform the numerical ED, which shows that the ground state of the fragmented cluster has, according to the Lieb-Mattis theorem [46], the total spin $S_{\text{total}} = \frac{n-1}{2}$. In this case, the contribution of the Zeeman term in Eq. (A1) can be singled out explicitly:

$$e_n(h) = \tilde{e}_n(h=0) - \frac{n-1}{2(n+1)}h + \frac{n}{n+1}J_2 - \frac{3}{4}J_2. \tag{A3}$$

The gapped Lieb-Mattis ferrimagnetic phase, which corresponds to the case of all triplet dimers (i.e., $n \to \infty$), has the following energy:

$$e_\infty(h) = \tilde{e}_\infty(h=0) - \tfrac{1}{2}h + J_2 - \tfrac{3}{4}J_2, \tag{A4}$$

where $\tilde{e}_\infty(h=0)$ denotes the ground-state energy of the mixed spin-$(\frac{1}{2}, 1)$ Heisenberg chain in zero field. The number n for which $e_n(h)$ attains the minimal value defines the period of the ground state for a particular set of parameters. It was proven that the MD phase set up the ground state for $J_2 > 2J_1$ [29]. For lower J_2, the TD state becomes favorable, and the boundary between both phases mentioned above is as follows:

$$J_2 = 2J_1 - h. \tag{A5}$$

The boundaries between the TD phase with period 2 and other high-periodic phases can be found by comparing their energies $e_1(h)$ and $e_n(h)$:

$$J_2^{(n)}(h) = h - \frac{2(n+1)}{n-1}[\tilde{e}_n(h=0) - J_1]. \tag{A6}$$

In Ref. [29], by the numerical ED of n coupled diamonds, it was found that $J_2^{(n)}(h=0) < J_2^{(n+1)}(h=0)$ for $n < 7$. It was imposed that $J_2^{(n)}$ monotonically increases with n up to infinity, which means that no other fragmented phases are possible in between the Lieb-Mattis and TD phases. Since all $J_2^{(n)}(h)$ depend identically on the field in Eq. (A6), the above arguments are also valid for the ground states in nonzero fields.

[1] C. Lacroix, P. Mendels, and F. Mila, *Introduction to Frustrated Magnetism: Materials, Experiment, Theory*, Springer Series in Solid-State Sciences (Springer, Heidelberg, 2010), Vol. 164.

[2] H. T. Diep, *Frustrated Spin Systems*, 3rd edition (World Scientific, Singapore, 2020).

[3] C. K. Majumdar and D. Ghosh, On next-nearest-neighbor interaction in linear chain, J. Math. Phys. **10**, 1388 (1969).

[4] B. S. Shastry and B. Sutherland, Exact ground state of a quantum mechanical antiferromagnet, Physica B+C **108**, 1069 (1981).

[5] F. Monti and A. Süto, Spin-$\frac{1}{2}$ Heisenberg model on Δ trees, Phys. Lett. A **156**, 197 (1991).

[6] M. P. Gelfand, Linked-tetrahedra spin chain: Exact ground state and excitations, Phys. Rev. B **43**, 8644 (1991).

[7] R. Schnalle and J. Schnack, Calculating the energy spectra of magnetic molecules: Application of real- and spin-space symmetries, Int. Rev. Phys. Chem. **29**, 403 (2010).

[8] J. Schnack, Effects of frustration on magnetic molecules: A survey from Olivier Kahn until today, Dalton Trans. **39**, 4677 (2010).

[9] J. Schnack and O. Wendland, Properties of highly frustrated magnetic molecules studied by the finite-temperature Lanczos method, Eur. Phys. J. B **78**, 535 (2010).

[10] O. Hanebaum and J. Schnack, Advanced finite-temperature Lanczos method for anisotropic spin systems, Eur. Phys. J. B **87**, 194 (2014).

[11] B. Schmidt and P. Thalmeier, Frustrated two dimensional quantum magnets, Phys. Rep. **703**, 1 (2017).

[12] P. Prelovšek and J. Kokalj, Finite-temperature properties of the extended Heisenberg model on a triangular lattice, Phys. Rev. B **98**, 035107 (2018).

[13] J. Schnack, J. Schulenburg, and J. Richter, Magnetism of the $N = 42$ kagome lattice antiferromagnet, Phys. Rev. B **98**, 094423 (2018).

[14] J. Schnack, J. Richter, and R. Steinigeweg, Accuracy of the finite-temperature Lanczos method compared to simple typicality-based estimates, Phys. Rev. Research **2**, 013186 (2020).

[15] A. Honecker, S. Wessel, R. Kerkdyk, T. Pruschke, F. Mila, and B. Normand, Thermodynamic properties of highly frustrated quantum spin ladders: Influence of many-particle bound states, Phys. Rev. B **93**, 054408 (2016).

[16] S. Wessel, B. Normand, F. Mila, and A. Honecker, Efficient quantum Monte Carlo simulations of highly frustrated magnets: The frustrated spin-$\frac{1}{2}$ ladder, SciPost Phys. **3**, 005 (2017).

[17] S. Wessel, I. Niesen, J. Stapmanns, B. Normand, F. Mila, P. Corboz, and A. Honecker, Thermodynamic properties of the Shastry-Sutherland model from quantum Monte Carlo simulations, Phys. Rev. B **98**, 174432 (2018).

[18] J. Stapmanns, P. Corboz, F. Mila, A. Honecker, B. Normand, and S. Wessel, Thermal Critical Points and Quantum Critical End Point in the Frustrated Bilayer Heisenberg Antiferromagnet, Phys. Rev. Lett. **121**, 127201 (2018).

[19] J. D'Emidio, S. Wessel, and F. Mila, Reduction of the sign problem near $T = 0$ in quantum Monte Carlo simulations, Phys. Rev. B **102**, 064420 (2020).

[20] L. Weber, A. Honecker, B. Normand, P. Corboz, F. Mila, and S. Wessel, Quantum Monte Carlo simulations in the trimer basis: First-order transitions and thermal critical points in frustrated trilayer magnets, SciPost Phys. **12**, 054 (2022).

[21] J. Schulenburg, A. Honecker, J. Schnack, J. Richter, and H.-J. Schmidt, Macroscopic Magnetization Jumps due to Independent Magnons in Frustrated Quantum Spin Lattices, Phys. Rev. Lett. **88**, 167207 (2002).

[22] M. E. Zhitomirsky and H. Tsunetsugu, High field properties of geometrically frustrated magnets, Prog. Theor. Phys. Suppl. **160**, 361 (2005).

[23] O. Derzhko and J. Richter, Universal low-temperature behavior of frustrated quantum antiferromagnets in the vicinity of the saturation field, Eur. Phys. J. B **52**, 23 (2006).

[24] O. Derzhko, J. Richter, and M. Maksymenko, Strongly correlated flat-band systems: The route from Heisenberg spins to Hubbard electrons, Int. J. Mod. Phys. B **29**, 1530007 (2015).

[25] J. Strečka, J. Richter, O. Derzhko, T. Verkholyak, and K. Karl'ová, Diversity of quantum ground states and quantum phase transitions of a spin-$\frac{1}{2}$ Heisenberg octahedral chain, Phys. Rev. B **95**, 224415 (2017).

[26] J. Strečka, J. Richter, O. Derzhko, T. Verkholyak, and K. Karl'ová, Magnetization process and low-temperature thermodynamics of a spin-$\frac{1}{2}$ Heisenberg octahedral chain, Phys. B: Condens. Matter **536**, 364 (2018).

[27] K. Karl'ová, J. Strečka, and T. Verkholyak, Cluster-based Haldane phases, bound magnon crystals and quantum spin liquids of a mixed spin-1 and spin-$\frac{1}{2}$ Heisenberg octahedral chain, Phys. Rev. B **100**, 094405 (2019).

[28] J. Strečka, O. Krupnitska, and J. Richter, Investigation of bipartite entanglement across the magnetization process of a highly frustrated spin-$\frac{1}{2}$ Heisenberg octahedral chain as a new paradigm of the localized-magnon approach, Europhys. Lett. **132**, 30004 (2020).

[29] K. Takano, K. Kubo, and H. Sakamoto, Ground states with cluster structures in a frustrated Heisenberg chain, J. Phys.: Condens. Matter **8**, 6405 (1996).

[30] H. Jeschke, I. Opahle, H. Kandpal, R. Valenti, H. Das, T. Saha-Dasgupta, O. Janson, H. Rosner, A. Bruhl, B. Wolf, M. Lang, J. Richter, Sh. Hu, X. Wang, R. Peters, T. Pruschke, and A. Honecker, Multistep Approach to Microscopic Models for Frustrated Quantum Magnets: The Case of the Natural Mineral Azurite, Phys. Rev. Lett. **106**, 217201 (2011).

[31] A. Honecker, S. Hu, R. Peters, and J. Richter, Dynamic and thermodynamic properties of the generalized diamond chain model for azurite, J. Phys.: Condens. Matter **23**, 164211 (2011).

[32] M. Fujihala, H. Koorikawa, S. Mitsuda, M. Hagihala, H. Morodomi, T. Kawae, A. Matsuo, and K. Kindo, Spin-liquid ground state in the spin $\frac{1}{2}$ distorted diamond chain compound $K_3Cu_3AlO_2(SO_4)_4$, J. Phys. Soc. Jpn. **84**, 073702 (2015).

[33] K. Morita, M. Fujihala, H. Koorikawa, T. Sugimoto, S. Sota, S. Mitsuda, and T. Tohyama, Static and dynamic magnetic properties of the spin-$\frac{1}{2}$ inequilateral diamond-chain compounds $A_3Cu_3AlO_2(SO_4)_4$ (A = K, Rb, Cs), Phys. Rev. B **95**, 184412 (2017).

[34] M. Fujihala, H. Koorikawa, S. Mitsuda, K. Morita, T. Tohyama, K. Tomiyasu, A. Koda, H. Okabe, S. Itoh, T. Yokoo, S. Ibuka, M. Tadokoro, M. Itoh, H. Sagayama, R. Kumai, and Y. Murakami, Possible Tomonaga-Luttinger spin liquid state in the spin-$\frac{1}{2}$ inequilateral diamond-chain compound $K_3Cu_3AlO_2(SO_4)_4$, Sci. Rep. **7**, 16785 (2017).

[35] W. Fujita, A. Tokumitu, Y. Fujii, and H. Kikuchi, Crystal growth, structures and magnetic properties of copper hydroxide compounds with distorted diamond chain magnetic networks, Cryst. Eng. Comm. **18**, 8614 (2016).

[36] M. Cui, N. Wang, S. Zhang, and Z. He, $Cu_3(CH_3COO)_4(OH)_2 \cdot 5H_2O$: A novel isolated spin-$\frac{1}{2}$ diamond chain compound showing possible valence-bond condensation, Cryst. Growth Des. **19**, 547 (2019).

[37] C. W. Liu, C.-M. Hung, B. Kumar Santra, J.-Ch. Wang, H.-M. Kao, and Zh. Lin, Ligand substitution in cubic clusters: Surprising isolation of the cocrystallization products of $Cu_8(\mu_8\text{-Se})[S_2P(OEt)_2]_6$ and $Cu_6[S_2P(OEt)_2]_6$, Inorg. Chem. **42**, 8551 (2003).

[38] S.-C. Xiang, S.-M. Hu, J.-J. Zhang, X.-T. Wu, and J.-Q. Li, A new spherical metallacryptate compound $[Na\{Cu_6(Thr)_8(H_2O)_2(ClO_4)_4\}].ClO_4.\ 5H_2O$: Magnetic properties and DFT calculations, Eur. J. Inorg. Chem. **2005**, 2706 (2005).

[39] X.-Q. Zhao, J. Wang, D.-X. Bao, S. Xiang, and D.-B. Luo, A high-nuclearity $[Cu_6Cd_4]$ antiferromagnet with a supertetrahedral configuration, Inorg. Chem. Commun. **62**, 77 (2015).

[40] X. Gao, S. He, C. Zhang, C. Du, X. Chen, W. Xing, S. Chen, A. Clayborne, and W. Chen, Single crystal sub-nanometer sized $Cu_6(SR)_6$ clusters: Structure, photophysical properties, and electrochemical sensing, Adv. Sci. **3**, 1600126 (2016).

[41] R. Robson, B. F. Abrahams, S. R. Batten, H. Hamit, and B. F. Hoskins, A cubic (3, 4)-connected net with large cavities in solvated $[Cu_3(tpt)_4](ClO_4)_3$ (tpt = 2, 4, 6-tri(4-pyridyl)- 1, 3, 5- triazine), Angew. Chem. Int. Ed. Engl. **35**, 1690 (1996).

[42] A. L. La Rooij, H. B. van Linden van den Heuvell, and R. J. C. Spreeuw, Designs of magnetic atom-trap lattices for quantum simulation experiments, Phys. Rev. A **99**, 022303 (2019).

[43] T. Verkholyak, J. Strečka, M. Jaščur, and J. Richter, Magnetic properties of the quantum spin-$\frac{1}{2}XX$ diamond chain: The Jordan-Wigner approach, Eur. Phys. J. B **80**, 433 (2011).

[44] O. Derzhko, J. Richter, A. Honecker, and H.-J. Schmidt, Universal properties of highly frustrated quantum magnets in strong magnetic fields, Low Temp. Phys. **33**, 745 (2007).

[45] O. Derzhko, J. Richter, and O. Krupnitska, Semiquantitative theory for high-field low-temperature properties of a distorted diamond spin chain, Condens. Matter Phys. **15**, 43702 (2012).

[46] E. Lieb and D. Mattis, Ordering energy levels of interacting spin systems, J. Math. Phys. **3**, 749 (1962).

[47] W. M. da Silva and R. R. Montenegro-Filho, Magnetic-field-temperature phase diagram of alternating ferrimagnetic chains: Spin-wave theory from a fully polarized vacuum, Phys. Rev. B **96**, 214419 (2017).

[48] J. Strečka, Breakdown of a magnetization plateau in ferrimagnetic mixed spin-($\frac{1}{2}$, S) Heisenberg chains due to a quantum phase transition towards the Luttinger spin liquid, Acta Phys. Pol. A **131**, 624 (2017).

[49] T. Verkholyak and J. Strečka, Magnetic signatures of quantum critical points of the ferrimagnetic mixed spin-($\frac{1}{2}$, S) Heisenberg chains at finite temperatures, J. Low. Temp. Phys. **187**, 712 (2017).

[50] W. M. da Silva and R. R. Montenegro-Filho, Role of density-dependent magnon hopping and magnon-magnon repulsion in ferrimagnetic spin-($\frac{1}{2}$, S) chains in a magnetic field, Phys. Rev. B **103**, 054432 (2021).

[51] N. B. Ivanov, J. Schnack, R. Schnalle, J. Richter, P. Kögerler, G. N. Newton, L. Cronin, Y. Oshima and H. Nojiri, Heat Capacity Reveals the Physics of a Frustrated Spin Tube, Phys. Rev. Lett. **105**, 037206 (2010).

[52] B. Bauer, L. D. Carr, H. G. Evertz, A. Feiguin, J. Freire, S. Fuchs, L. Gamper, J. Gukelberger, E. Gull, S. Guertler, A. Hehn, R. Igarashi, S. V. Isakov, D. Koop, P. N. Ma, P. Mates, H. Matsuo, O. Parcollet, G. Pawlowski, J. D. Picon *et al.*, The ALPS project release 2.0: Open source software for strongly correlated systems, J. Stat. Mech. (2011) P05001.

[53] H. A. Kramers and G. H. Wannier, Statistics of the two-dimensional ferromagnet. Part I, Phys. Rev. **60**, 252 (1941).

[54] J. Richter and J. Schulenburg, The spin-$\frac{1}{2}$ J_1-J_2 Heisenberg antiferromagnet on the square lattice: Exact diagonalization for $N = 40$ spins, Eur. Phys. J. B **73**, 117 (2010).

[55] J. Schulenburg, SPINPACK, http://www-e.uni-magdeburg.de/jschulen/spin/.

[56] H. Niggemann, G. Uimin, and J. Zittartz, Mixed Heisenberg chains: II. Thermodynamics, J. Phys.: Condens. Matter **10**, 5217 (1998).

[57] K. Hida, K. Takano, and H. Suzuki, Finite temperature properties of mixed diamond chain with spins 1 and $\frac{1}{2}$, J. Phys. Soc. Jpn. **78**, 084716 (2009).

[58] J. Schulenburg, and J. Richter, Infinite series of magnetization plateaus in the frustrated dimer-plaquette chain, Phys. Rev. B **65**, 054420 (2002).

[59] K. Hida, Infinite series of ferrimagnetic phases emergent from the gapless spin liquid phase of mixed diamond chains, J. Phys. Soc. Jpn. **90**, 054701 (2021).